pharmaceuticals

MDPI

Article

Inhibiting *Leishmania donovani* Sterol Methyltransferase to Identify Lead Compounds Using Molecular Modelling

Patrick O. Sakyi [1,2], Samuel K. Kwofie [3,4,*], Julius K. Tuekpe [4], Theresa M. Gwira [4], Emmanuel Broni [3,5,6], Whelton A. Miller III [6,7,8], Michael D. Wilson [5,6] and Richard K. Amewu [1,*]

1 Department of Chemistry, School of Physical and Mathematical Sciences, College of Basic and Applied Sciences, University of Ghana, Legon, Accra P.O. Box LG 56, Ghana
2 Department of Chemical Sciences, School of Sciences, University of Energy and Natural Resources, Sunyani P.O. Box 214, Ghana
3 Department of Biomedical Engineering, School of Engineering Sciences, College of Basic & Applied Sciences, University of Ghana, Legon, Accra P.O. Box LG 77, Ghana
4 Department of Biochemistry, Cell, and Molecular Biology, West African Centre for Cell Biology of Infectious Pathogens, College of Basic and Applied Sciences, University of Ghana, Accra P.O. Box LG 54, Ghana
5 Department of Parasitology, Noguchi Memorial Institute for Medical Research (NMIMR), College of Health Sciences (CHS), University of Ghana, Legon, Accra P.O. Box LG 581, Ghana
6 Department of Medicine, Loyola University Medical Center, Maywood, IL 60153, USA
7 Department of Molecular Pharmacology and Neuroscience, Loyola University Medical Center, Maywood, IL 60153, USA
8 Department of Chemical and Biomolecular Engineering, School of Engineering and Applied Science, University of Pennsylvania, Philadelphia, PA 19104, USA
* Correspondence: skkwofie@ug.edu.gh (S.K.K.); ramewu@ug.edu.gh (R.K.A.); Tel.: +233-203797922 (S.K.K.); +233-543823483 (R.K.A.)

Abstract: The recent outlook of leishmaniasis as a global public health concern coupled with the reportage of resistance and lack of efficacy of most antileishmanial drugs calls for a concerted effort to find new leads. The study combined *In silico* and in vitro approaches to identify novel potential synthetic small-molecule inhibitors targeting the *Leishmania donovani* sterol methyltransferase (*Ld*SMT). The *Ld*SMT enzyme in the ergosterol biosynthetic pathway is required for the parasite's membrane fluidity, distribution of membrane proteins, and control of the cell cycle. The lack of *Ld*SMT homologue in the human host and its conserved nature among all *Leishmania* parasites makes it a viable target for future antileishmanial drugs. Initially, six known inhibitors of *Ld*SMT with $IC_{50} < 10$ μM were used to generate a pharmacophore model with a score of 0.9144 using LigandScout. The validated model was used to screen a synthetic library of 95,630 compounds obtained from InterBioScreen limited. Twenty compounds with pharmacophore fit scores above 50 were docked against the modelled three-dimensional structure of *Ld*SMT using AutoDock Vina. Consequently, nine compounds with binding energies ranging from −7.5 to −8.7 kcal/mol were identified as potential hit molecules. Three compounds comprising STOCK6S-06707, STOCK6S-84928, and STOCK6S-65920 with respective binding energies of −8.7, −8.2, and −8.0 kcal/mol, lower than 22,26-azasterol (−7.6 kcal/mol), a known *Ld*SMT inhibitor, were selected as plausible lead molecules. Molecular dynamics simulation studies and molecular mechanics Poisson–Boltzmann surface area calculations showed that the residues Asp25 and Trp208 were critical for ligand binding. The compounds were also predicted to have antileishmanial activity with reasonable pharmacological and toxicity profiles. When the antileishmanial activity of the three hits was evaluated in vitro against the promastigotes of *L. donovani*, mean half-maximal inhibitory concentrations (IC_{50}) of 21.9 ± 1.5 μM (STOCK6S-06707), 23.5 ± 1.1 μM (STOCK6S-84928), and 118.3 ± 5.8 μM (STOCK6S-65920) were obtained. Furthermore, STOCK6S-84928 and STOCK6S-65920 inhibited the growth of *Trypanosoma brucei*, with IC_{50} of 14.3 ± 2.0 μM and 18.1 ± 1.4 μM, respectively. The identified compounds could be optimised to develop potent antileishmanial therapeutic agents.

Keywords: *Leishmania donovani*; sterol methyltransferase; pharmacophore; ergosterol biosynthesis; molecular docking; molecular dynamics simulation; in vitro studies

Citation: Sakyi, P.O.; Kwofie, S.K.; Tuekpe, J.K.; Gwira, T.M.; Broni, E.; Miller, W.A., III; Wilson, M.D.; Amewu, R.K. Inhibiting *Leishmania donovani* Sterol Methyltransferase to Identify Lead Compounds Using Molecular Modelling. *Pharmaceuticals* **2023**, *16*, 330. https://doi.org/10.3390/ph16030330

Academic Editor: Osvaldo Andrade Santos-Filho

Received: 19 October 2022
Revised: 3 February 2023
Accepted: 7 February 2023
Published: 21 February 2023

1. Introduction

The challenges associated with control coupled with the frequent epidemic outbreak have rendered leishmaniasis an important public health problem [1–3]. Consequently, the presence of the ugly lesions after treatment and the severity of those caused by *Leishmania donovani* and *Leishmania infantum* in humans has rendered visceral leishmaniasis a global public health concern that needs urgent attention [1,3]. Currently, there are no vaccines and the number of chemotherapeutic options is limited [4,5]. Drugs including pentamidine, amphotericin B, paromomycin, miltefosine, and stibogluconate are ineffective and toxic, and the parasite has developed resistance, requiring renewed and concerted efforts to identify and develop new antileishmanial chemotypes [6,7]. Some efforts have been made towards finding new treatment options from natural products [8,9]; however, their structures and chemical synthesis are complex [10,11].

Synthetic small molecules with drug-like properties have been explored for the treatment of various ailments including leishmaniasis [12,13]. Recent studies show that about 60% of the drugs used for treating most diseases originated from synthetic small molecules [14,15]. The inherent properties of synthetic small molecules such as the ability to cross biological barriers and to modulate diverse biological targets render them viable drug candidates [16].

Target identification and validation are pivotal in drug design and the success of drug development depends primarily on choosing the right target. Studies in the design of antileishmanial compounds have identified some novel pathways and protein targets necessary for the parasite's survival [17,18]. Some of these targets have been validated [19,20], while investigation on others is still ongoing. Ergosterol biosynthesis is involved in various biological functions including plasma membrane formation, membrane fluidity, distribution of membrane proteins, and control of the cell cycle [21]. Ergosterol is essential for optimal mitochondrion function in *Leishmania* parasites [22]. This pathway is catalysed by several enzymes with homologues in the human host and hence has the potential to cause off-target effects, mainly as a result of poor selectivity [23]. Sterol methyltransferase, which catalyses the transfer of the methyl group from S-adenosine-methionine to the C24 position of the sterol side chain during ergosterol biosynthesis, lacks a homologue in humans [22,24], and is thus considered an essential drug target.

Reports have shown that 22,26-azasterol suppresses the growth of *L. donovani* with a half-maximal inhibitory concentration (IC_{50}) of 8.9 μM [25]. To improve the inhibitory effect of 22,26-azsterol, some analogues (Figure 1) were generated, and their activities were found to be dependent on the presence of ammonium or sulfonium functionality in the side chain [25]. Similarly, ezetimibe, imipramine, and simeprevir (Figure 1) have shown promising inhibitory activity against *L. donovani* by making morphological changes to the plasma and mitochondrion membranes with IC_{50} of 30, 28.6, and 51.49 μM, respectively [26–28]. A fragment-based de novo design was used to predict potential inhibitors against *L. donovani* sterol methyltransferase (*Ld*SMT) [29]. Though several hit compounds have been identified targeting this enzyme, only a few progressed to the clinical evaluation stage [30–34].

In silico techniques offer alternative platforms for the identification of novel hits in a timely and cost-effective manner [35,36]. These approaches have improved rational drug design and augmented the identification of potentially new drug candidates. This study, therefore, employs ligand-based pharmacophore virtual screening, molecular docking, molecular dynamics (MD) simulations, molecular mechanics Poisson–Boltzmann surface area (MM/PBSA), biological activity predictions, and in vitro studies to support the identification of potential inhibitors. The synthetic compound library was screened against *Ld*SMT followed by the elucidation of the mechanisms of binding of the proposed molecules.

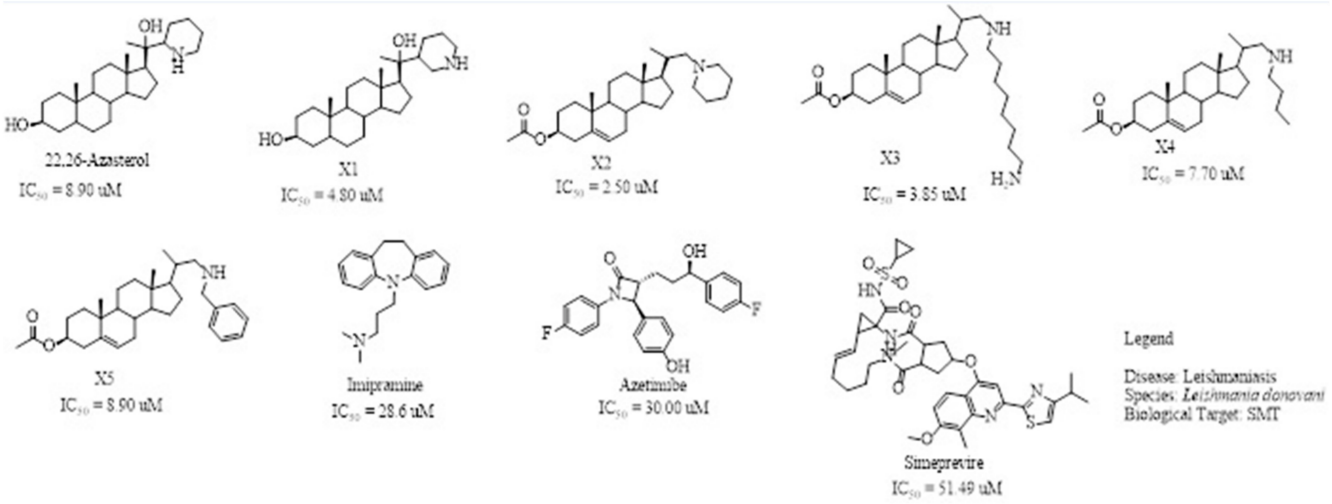

Figure 1. Chemical structures of some known inhibitors of *Leishmania donovani* sterol methyltransferase and their IC_{50} values. The biological target is sterol methyltransferase (SMT).

2. Materials and Methods

The schematic workflow employed in the project is shown in Figure 2. First, six known inhibitors of *Ld*SMT with IC_{50} less than 10 µM were used to generate a pharmacophore model employing the merged feature embedded in LigandScout version 4.3 [37]. The pharmacophore model was then used to screen a library of 95,630 synthetic compounds from InterBioScreen limited. Ligands with pharmacophore fit scores above 50 were docked against a previously modelled structure of *Ld*SMT [29,38]. The selected hit compounds were evaluated via physicochemical, pharmacological, and toxicity profiles, as well as biological activity predictions, MD simulations, and MM/PBSA computations. Three potential lead compounds were then screened in vitro to validate the *In silico* studies.

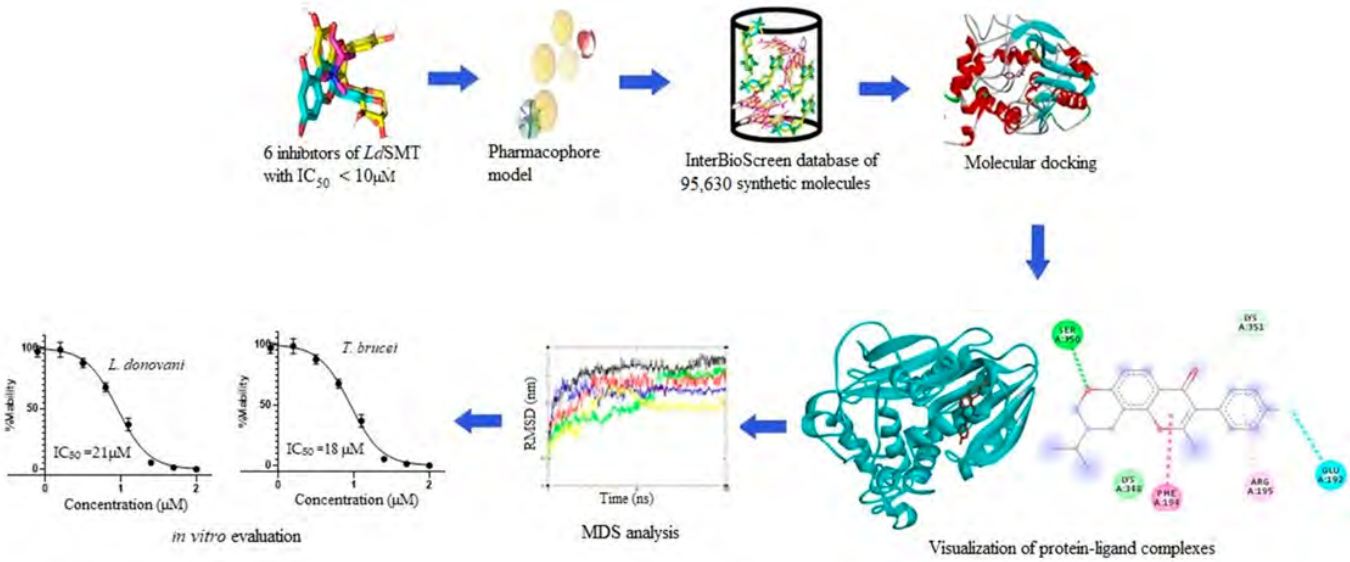

Figure 2. Methodology schema employed in the identification of antileishmanial compounds targeting *Ld*SMT. The workflow details the pharmacophore-based virtual screening, molecular docking, and MD simulation as well as in vitro validation of the selected potential antileishmanial and antitrypanosomal chemotypes.

2.1. Target Preparation

The three-dimensional (3D) structure of *Ld*SMT previously elucidated using Modeller version 10.2 [29,38] was used. Energy minimisation of the target protein was carried out

by employing the Optimized Potential for Liquid Simulations (OPLS)/All Atom force field [39] via the Groningen Machine for Chemical Simulations GROMACS version 2018 (GROMACS 2018) [40,41]. Biovia Discovery Studio Visualizer v.19.1.0.18287 [42] was used to visualise the energy-minimised structure, remove water molecules, and solvate the protein, and then the result was saved in Protein Data Bank (pdb) format, which was later converted to AutoDock Vina's [43] compatible pdbqt format.

2.2. Binding Site Prediction

The amino acid residues and the probable volume and area of the binding site of the modelled protein were determined using the Computed Atlas of Surface Topography of proteins (CASTp) [44] and Biovia Discovery Studio Visualizer v.19.1.0.18287 [42], as indicated in a previous study [29].

2.3. Ligand-Based Pharmacophore Virtual Screening

Six of the known inhibitors (Figure 1) of *Ld*SMT with IC_{50} less than 10 µM were employed in generating the pharmacophore model using LigandScout version 4.3 [37]. The structure data file (sdf) formats of the ligands were used via LigandScout's Ligand-Based Modeling Perspective v.4.3 [37]. The default settings of OMEGA best were used to generate a maximum of 200 conformations per ligand.

2.4. Retrieval and Preparation of Chemical Library for Pharmacophore-Based Screening

A chemical library of 95,630 synthetic compounds was retrieved from InterBioScreen limited [45] and used for the pharmacophore-based virtual screening.

2.5. Pharmacophore-Based Virtual Screening of the Libraries

The 95,630 chemical entities retrieved from InterBioScreen limited were utilised for the pharmacophore screening using LigandScout v.4.3 [46], first by converting from "sdf" to "lbd" and then by screening against a validated pharmacophore model.

2.6. Validation of Pharmacophore Model and AutoDock Vina

Before performing the virtual screening, both the pharmacophore model and AutoDock Vina v.1.2.0 [43] were validated to assess their potential for distinguishing between active compounds and decoys.

2.6.1. Pharmacophore Model Validation

The receiver operating characteristic (ROC) curve and enrichment factors (EFs) were used in validating the pharmacophore model in LigandScout v.4.3 [37]. The six inhibitors of SMT and their decoys were used to generate the ROC curve from where the area under the curve (AUC) and EFs were calculated.

2.6.2. Validation of AutoDock Vina

The simplified molecular input line entry system (SMILES) of six of the known inhibitors with IC_{50} less than 10 µM served as active compounds for the generation of 50 decoys each using the Directory of Useful Decoys (DUD-E) [47]. The ROC curves generated via EasyROC v.1.3.3 [48] were used to validate the docking protocol of AutoDock Vina v.1.2.0 [43].

2.7. Molecular Docking Studies of Chemical Entities with Good Pharmacophore Fit Scores

AutoDock Vina [43] interfaced with PyRx v.0.8 [49], which employs empirical scoring functions, was used for the virtual screening. Ligands with good pharmacophore fit scores were obtained after screening the pharmacophore model against the library combined with 22,26-azasterol and the three known drugs (amphotericin B, miltefosine, and paromomycin). The energy-minimised protein (*Ld*SMT) was used for molecular docking via AutoDock Vina v.1.2.0 [43]. The charge, hydrogen bond network, and histidine proto-

nation state of the protein were assigned after pdbqt conversion [32]. The grid box size (91.445 × 73.502 × 78.352) Å^3 with the centre (72.200, 58.009, 13.302) Å was used with an exhaustiveness of 8 [29].

2.8. Characterisation of Mechanism of Binding

Biovia Discovery Studio Visualizer v.19.1.0.18287 [42] was employed in the elucidation of the protein–ligand interactions.

2.9. ADMET Properties and Drug-Likeness Assessment

The absorption, distribution, metabolism, excretion, and toxicity (ADMET) properties were determined using SwissADME [50] and the OSIRIS Property Explorer in DataWarrior [51]. This was carried out to evaluate the drug-likeness and the pharmacologic properties of the selected compounds.

2.10. Prediction of Biological Activity of Selected Compounds

The biological activity of the compounds was predicted using Prediction of Activity Spectra for Substance (PASS) [52]. The SMILES files of the molecules were used as inputs.

2.11. Molecular Dynamics Simulation Analyses of Protein and Protein–Ligand Complexes

A 100 ns MD simulation was adopted [29] for *Ld*SMT and *Ld*SMT–ligand complexes via a sample interval for configuration of 100 ps using GROMACS 2018 [40,41]. Initially, the topology and position restrain files for the protein were generated using OPLS/All Atom force field [39]. LigParGen [53] was employed to generate the topology and parameter files of the ligands. The unbound protein and protein–ligand complexes were centred in a cubic simulation box with a 1 nm distance from the edges to restrain particle movements that have the potential to cause effects on the surface atoms [54]. System solvation was carried out using a single-point charge and then neutralised to achieve a molarity of 0.15 M using NaCl. Each system was energy-minimised for 50,000 steps using the steepest descent method. A 100 ps equilibration was carried out using several substances, volume and temperature, and several substances, pressure, and temperature ensembles [54] to ensure a well-equilibrated system was achieved at 300 K and a pressure of 1 bar. The root-mean-square deviation (RMSD), root-mean-square fluctuation (RMSF), the radius of gyration (Rg), and surface accessible surface area (SASA) trajectories were plotted using Qtgrace [55]. MM/PBSA computations of the complexes were carried out using g_MM/PBSA, which calculates the free binding energy and the individual energy contributions of the residues [56].

2.12. Parasite Culture and In Vitro Effect of Compounds on L. donovani Promastigotes

L. donovani promastigotes (MHOM/SD/62/1S strain—Bei Resources NIAID, NIH) were used for the cell viability assay. The promastigotes were grown at 25 °C in M199 medium supplemented with 10% heat-inactivated foetal bovine serum, penicillin G sodium (100 g/mL), and streptomycin sulphate (100 g/mL), and subcultured every 72 h in the same medium at a density of 2 × 10^5 cells/mL.

To determine the concentration of a compound that inhibits the growth of 50% (IC_{50}) of the *Leishmania* parasite population, promastigotes at a density of 2 × 10^5 cells were incubated in triplicate without or with the compounds at varying concentrations (100–0.781) µg/mL and kept at 25 °C for 72 h. The Alamar blue test was used to determine the vitality of the parasites as previously described [57]. At an excitation wavelength of 530 nm and an emission wavelength of 590 nm, fluorescence was measured using a Varioskan Lux Elisa microplate reader (Thermo Fisher Scientific, Waltham, MA, USA). The fluorescence counts were plotted against drug concentrations, and the IC_{50} was calculated using a dose–response curve via GraphPad Prism version 9 (GraphPad Software Inc., San Diego, CA, USA). The reference drug used in the assay is amphotericin B, a known drug for treating leishmaniasis.

2.13. In Vitro Culture and Cell Viability Assay for Trypanosoma brucei brucei GUTat 3.1

Similar to the approach described in Section 2.12, to determine the IC_{50} of the compounds against *Trypanosoma brucei brucei* GUTat 3.1 parasite population, the modifications were *trypanosomes* at a density of 4×10^3 cells, which were kept at 37 °C for 72 h [58]. The control drug used for this assay was diminazene aceturate (Sigma-Aldrich, Kent, UK), a veterinary drug used to combat infections of *trypanosomes* in cattle.

3. Results and Discussion

The results from the study are presented in the following sections, including the pharmacophore-based design, molecular docking, ADMET profiling, prediction of biological activities of selected molecules, MD simulations, MM/PBSA computations, and biological activity evaluations.

3.1. Predictions of LdSMT Binding Site Residues

A binding site is a pocket or groove on a protein that serves as a site for a ligand or biological macromolecule to bind with specificity. Ligands bind at active sites to induce biochemical reactions including methylation, demethylation, and phosphorylation. CASTp [44], which employs Delaunay triangulation, alpha shape, and discrete flow methods to identify topographic features and measure areas and volumes, was used to predict the binding site of *Ld*SMT in previous work [29]. The predicted binding site volume was 446.632 $Å^3$ and the area was 905.262 $Å^2$, and the critical amino acid residues elucidated included Ala30, Asp108, Val109, Tyr206, Gly207, Trp208, Met210, Tyr220, Tyr275, Leu278, Glu324, Ser328, Leu329, Val330, and Val331 [29].

3.2. Pharmacophore Generation

For pharmacophore generation and the prediction of features, six *Ld*SMT inhibitors (22,26-azasterol and X1-X5) (Figure 1) with IC_{50} < 10 μM were used. In addition, all six ligands and their decoys were employed to validate the pharmacophore model using the merged feature of LigandScout version 4.3 [37], similar to previous studies [59]. A predicted score of 0.9144 was generated with features consisting of three hydrophobic interactions (H), one positive ionisable (PI), one hydrogen bond acceptor (HBA), and one hydrogen bond donor (HBD) (Figure 3).

3.3. Validation of Generated Pharmacophore Model

The ROC curve evaluates the ability of the model to efficiently distinguish between a compendium of active and inactive compounds [59]. The ROC curve was obtained by plotting a graph of 1—specificity (Equation (1)) on the *x*-axis against sensitivity (obtained using Equation (2)) on the *y*-axis [60]. Notably, 1—specificity is called false positive fraction (FPF) and the sensitivity is also known as the true positive fraction (TPF).

$$\mathrm{FPF} = \frac{\mathrm{FP}}{(\mathrm{FP} + \mathrm{TN})} \tag{1}$$

$$\mathrm{TPF} = \frac{\mathrm{TP}}{(\mathrm{TP} + \mathrm{FN})} \tag{2}$$

where FP denotes false positive, TN as true negative, TP as true positive, and FN as false negative.

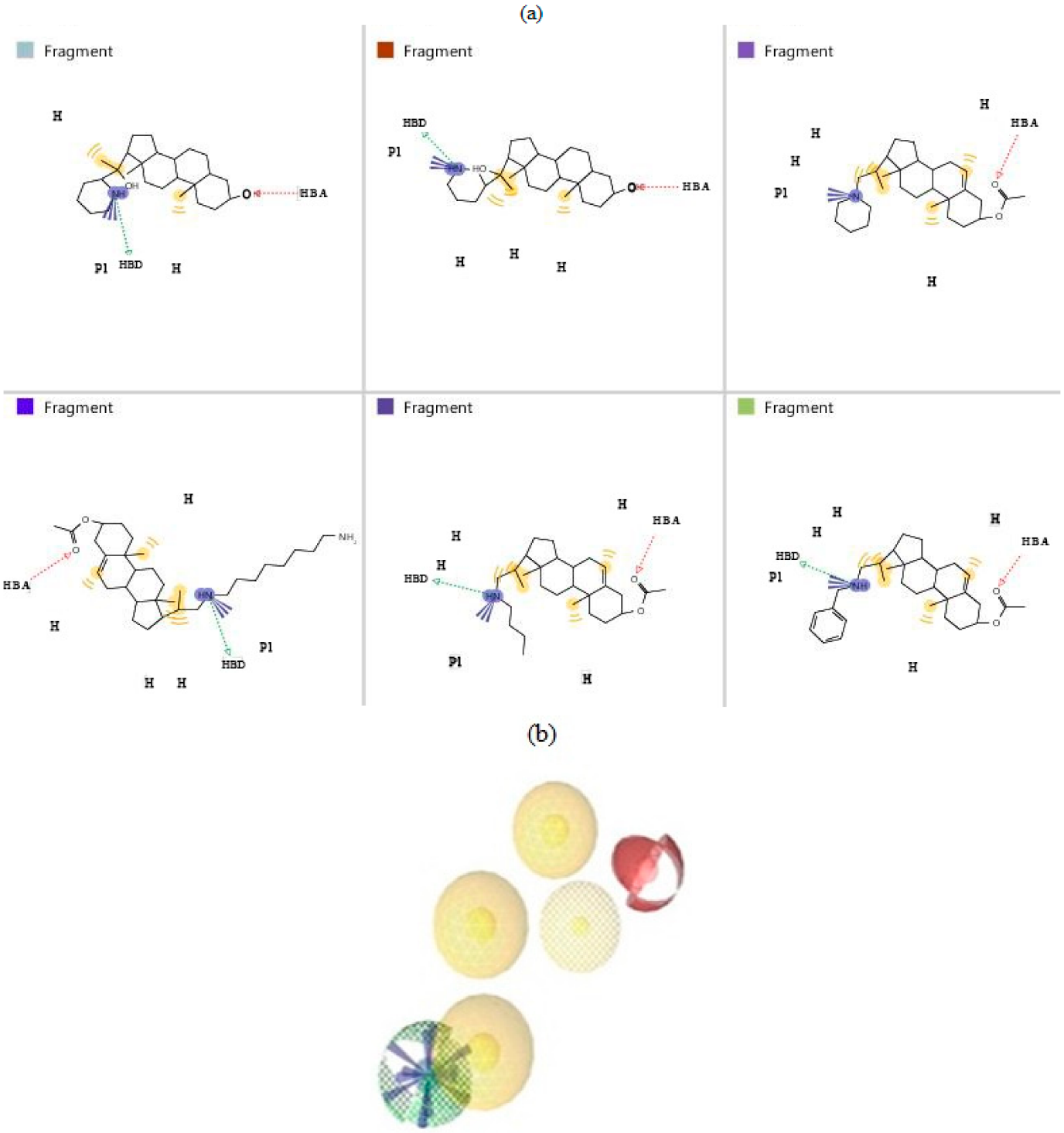

Figure 3. Pharmacophore features generated from (**a**) the six ligands comprising H, PI, HBA, and HBD; and (**b**) the pharmacophore model produced from merging the pharmacophore descriptors of all six inhibitors. Red balls indicate HBA, yellow balls denote H, green regions show HBD, and blue regions represent PI.

Consequently, while a poor test has a ROC curve falling on the diagonal line, a perfect test has the ROC curve passing through the upper left corner with approximately 100% sensitivity and 100% specificity [60]. The ROC curve (Figure 4a) falls to the upper left corner, implying a reasonably valid pharmacophore model. The AUC ranges from 0 to 1, with values close to 1 signifying a perfect model with the ability to distinguish active

from inactive compounds [59]. The six known inhibitors serving as active compounds were used to generate 300 decoys made up of 50 decoys from each. A total of 306 compounds comprising six active molecules and 300 decoys were screened via the 3D pharmacophore model and the AUC was computed as 1 (Figure 4a). The pharmacophore-guided approach was used to identify inhibitors of *Mycobacterium ulcerans* Cystathione γ-synthase MetB and an AUC of 0.7 was obtained after validation [59]. In addition, EF, which is the ratio of the number of identified active compounds within a pool of highly ranked hits to those randomly selected from the original dataset, was computed to evaluate the effectiveness of the pharmacophore model [61,62]. The EF was computed using Equation (3) [61].

$$EF = (N_{hits\ sampled}/N_{sampled})/(N_{total\ hits}/N_{total}) \quad (3)$$

where $N_{hits\ sampled}$ is the number of identified true hits in the hit list, $N_{sampled}$ is the number of compounds in the hit list, $N_{total\ hits}$ is the number of hits in the dataset, and N_{total} is the total number of compounds in the dataset.

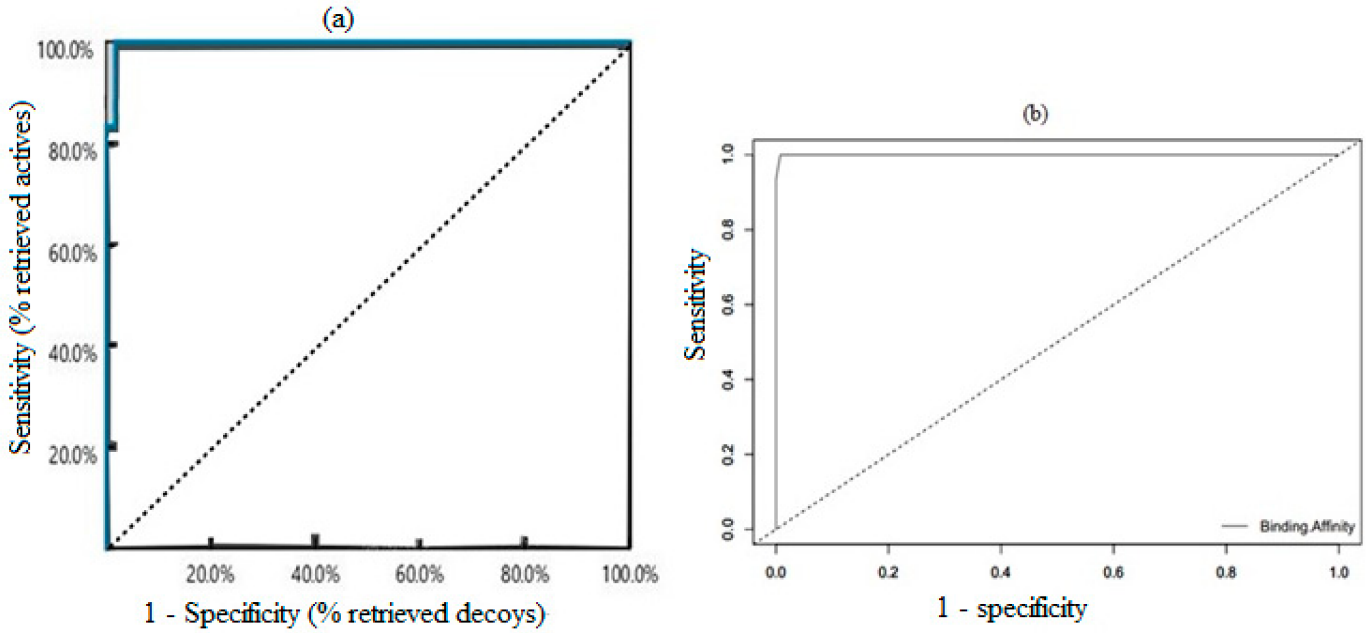

Figure 4. ROC curves for validation of the pharmacophore model and the docking protocols. (**a**) ROC curve of the selected pharmacophore model showing both the AUCs and EFs as measured in the top 1%, 5%, 10%, and 100% to be 52.0, 26.0, 26.0, and 26.0, respectively. (**b**) ROC curve generated after docking six active compounds and 300 decoys. The further away the median (that is, the dotted line) is from the curve, the better the model.

A pharmacophore model with EF less than 1 suggests the classification ability is low. Similarly, EF equal to one shows that the model has equal chances of classifying active and inactive compounds. In addition, an EF greater than one suggests the model has a greater potential of classifying active compounds. A pharmacophore model generated for the design of sigma-1 ligands was classified as poor due to the computed EF being close to 1 at 10% [63]. Similarly, a model with EF score above 1 classified the inhibitors significantly better [61]. Consequently, the EFs were obtained as 52.0, 26.0, 26.0, and 26.0 for 1%, 5%, 10%, and 100%, respectively, implying the effectiveness of the pharmacophore model in classifying hits amongst the dataset.

3.4. Validation of Docking Protocol

Most docking algorithms, including the Lamarckian genetic algorithm and the empirical scoring for free energy binding employed in AutoDock Vina, sometimes fail to accurately predict the pose and scoring functions, warranting validation [64]. The com-

puted AUC under the ROC was used to evaluate the performance of AutoDock Vina v.1.2.0 [43] in distinguishing the active from inactive compounds. To validate the docking protocol, the six active compounds and 300 decoys were virtually screened against the *Ld*SMT to generate the ROC curve and the AUC was computed as 0.9997 (Figure 4b) [65,66]. The ROC curve (Figure 4b) aligns with the upper left corner of the graph, which signifies a reasonably excellent docking protocol. The AUC of 0.9997 suggests that AutoDock Vina v.1.2.0 [43] has a plausible ability to distinguish active compounds from decoys.

3.5. Pharmacophore-Based Virtual Screening of Library

Pharmacophore-based virtual screening is the generation of a 3D query by exploring the chemical features responsible for the biological activity from a reasonable number of structures for the identification of new chemotypes [67,68]. The surge in interest is due to the high enrichment of novel actives generated from a library of chemical entities [67]. The validated pharmacophore model was used as a 3D query to screen a chemical library of 95,630 synthetic compounds from InterBioScreen limited with a pharmacophore fit score of 50 as the threshold. STOCK6S-64914 and STOCK6S-47366 had the highest and least pharmacophore fit scores of 59.39 and 57.15, respectively, among the 20 shortlisted compounds (Table 1).

Table 1. Selected compounds with pharmacophore fit scores above 50 via pharmacophore-based virtual screening.

Compound ID	Pharmacophore Fit Score	Compound ID	Pharmacophore Fit Score
STOCK6S-64941	59.39	STOCK6S-14893	58.37
STOCK6S-43563	59.23	STOCK6S-06707	58.24
STOCK6S-07535	59.19	STOCK7S-11482	58.14
STOCK6S-33909	59.19	STOCK6S-16994	58.05
STOCK6S-39547	59.18	STOCK6S-64616	57.53
STOCK6S-19430	59.00	STOCK6S-65229	57.44
STOCK7S-75883	58.89	STOCK6S-63483	57.37
STOCK7S-14941	58.87	STOCK6S-55084	57.33
STOCK6S-84928	58.85	STOCK6S-65920	57.3
STOCK6S-47549	58.47	STOCK6S-47366	57.15

3.6. Molecular Docking Analysis

Molecular docking predicts the orientation and conformation of the ligand within the binding site of the target protein. Strategically, molecular docking is supposed to mimic a biological system, but being a computational-based approach [69], it often suffers certain drawbacks. In the current study, the effects and implications of solvent present in the protein that otherwise may affect the pose of the ligand [70] were not considered, as water molecules were deleted during protein preparation. MD simulation studies were carried out to ascertain the contribution of the solvent in the free binding energy of the protein–ligand complexes similar to previous studies [71,72]. In addition, the preparations of both the protein and the ligand before docking have the potential to introduce errors, leading to missing bonds and abnormal geometries. This occurs when converting from pdb or sdf to the AutoDock Vina format pdbqt. Visualisation analysis of the protein and ligands after preparation and file conversion before docking ensures that this does not affect the pose of the ligands. The exhaustiveness in the current study was set to default 8, which statistically may not represent the actual number of possible conformations of ligands in the binding pocket of the biological target. This is normally occasioned to save computational time and energy. Furthermore, the top-ranked pose was chosen as the best pose with the least binding energy. Interestingly, this is not always the case, as the top-ranked score may not necessarily represent the best pose. Despite these drawbacks, molecular docking has provided an ideal platform for studying molecular inclusions at the atomic level [73].

Molecular docking has been explored in the identification of lead compounds including gentisic acid 5-O glucoside [59], simeprevir [28], and bisindolylmaleimide IX [74] by targeting Buruli ulcer [59], visceral leishmaniasis [28], and SARS-CoV-2 [74], respectively. In all these instances, the binding energies associated with the protein–ligand complexes were used as part of the criteria to shortlist the hits. The 20 shortlisted compounds from the pharmacophore screening were docked into the catalytic domain [29] of the *Ld*SMT structure with binding energies comparable to or lower than that of 22,26-azasterol (−7.6 kcal/mol). The binding energies of nine compounds (Table 2) were also lower than those of the antileishmanial drugs amphotericin B (−5.3 kcal/mol), miltefosine (−5.0 kcal/mol), and paromomycin (−4 kcal/mol) (Table 2). The binding energies ranged from −7.5 to −8.7 kcal/mol with STOCK6S-07353, STOCK6S-16994, and STOCK6S-06707 having −7.5, −7.5, and −8.7 kcal/mol, respectively. The results showed that the nine selected compounds possess better binding energies and can be explored as further potential inhibitors.

Table 2. Binding energies of the selected compounds after molecular docking with generated intermolecular bonds.

Ligands	Binding Energy/kcal/mol	Binding Residues	
		Hydrogen Bonds	Hydrophobic Bonds
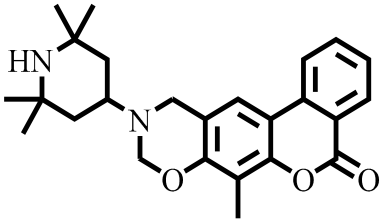 STOCK6S-06707	−8.7		Asp25, Ala28, Asp31, Arg32, Phe307, Ala311
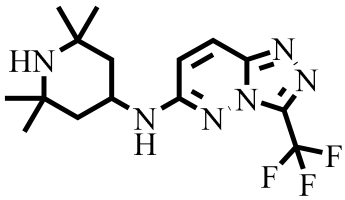 STOCK6S-84928	−8.2	Arg15, Asp28, Arg227	Leu13, Lys313
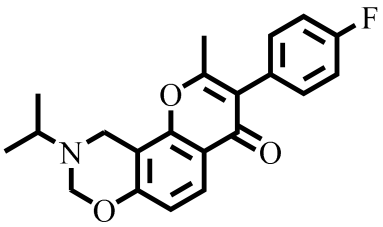 STOCK6S-65920	−8.0	Ser350	Glu192, Phe194, Arg195, Lys351

Table 2. *Cont.*

Ligands	Binding Energy/kcal/mol	Binding Residues	
		Hydrogen Bonds	**Hydrophobic Bonds**
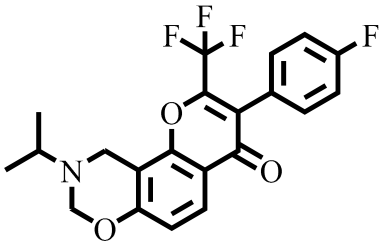 STOCK6S-55084	−7.9		Glu178, Trp208, His226, Ile228
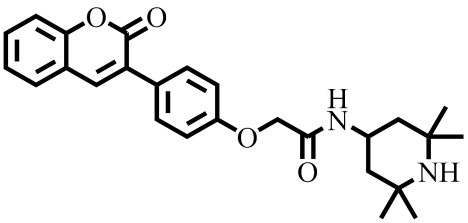 STOCK6S-64941	−7.8	Asp281, Ser284	Leu322
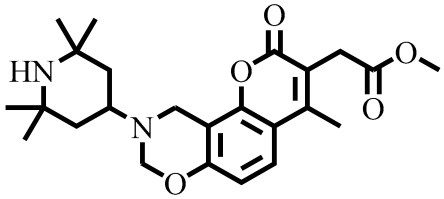 STOCK6S-19430	−7.7	Arg289, Arg295	Tyr316, Glu320
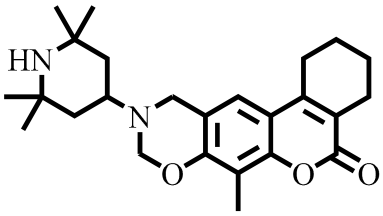 STOCK65-14893	−7.6		Ala28, Phe307, Val308, Ala311
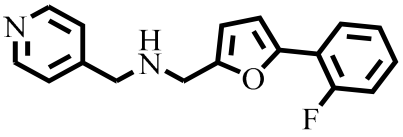 STOCK6S-07353	−7.5	Glu219, Glu229, Tyr275	Trp208, Ile224, Lys225, Ile228, Ile272
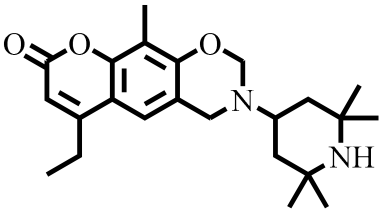 STOCK6S-16994	−7.5	Thr338	Phe93, Ile258

Table 2. *Cont.*

Ligands	Binding Energy/kcal/mol	Binding Residues	
		Hydrogen Bonds	Hydrophobic Bonds
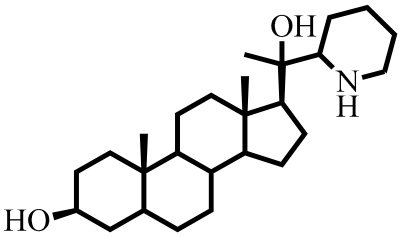 22,26-Azasterol	−7.6	Glu102, Gly200	Phe100, Lys198, Pro199
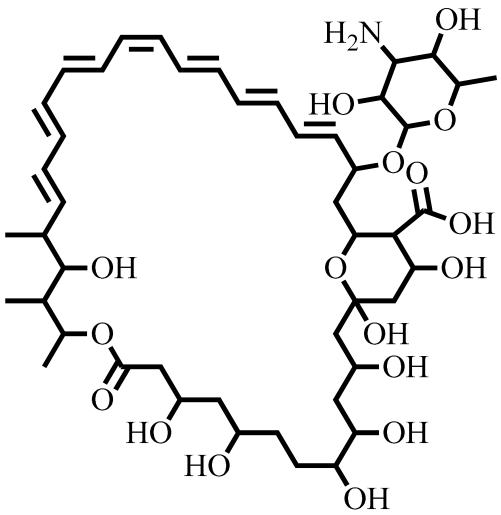 Amphotericin B	−5.3	Arg309, Asn299, Gly294, Leu288	
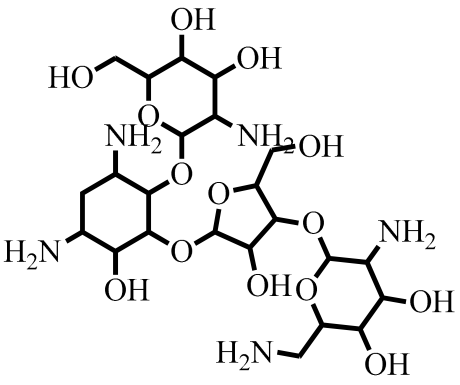 Paromomycin	−5.0	Asp31, Arg32, Val308, Arg309, Leu310	Glu306

Table 2. *Cont.*

Ligands	Binding Energy/kcal/mol	Binding Residues	
		Hydrogen Bonds	Hydrophobic Bonds
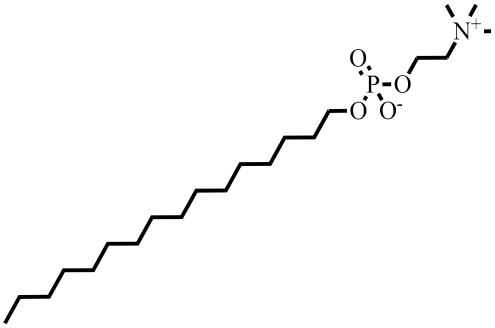 Miltefosine	−4.0	Cys202	Phe100, Met101, Asp104, Asp172, Pro199, Gly200, Thr201, Tyr343, Ile344

3.7. Protein–Ligand Interaction

Molecular recognition due to protein–ligand interactions is the basis of most cellular mechanisms. The examination of this at the atomistic level provides insights into the design of small-molecule drugs. Molecular docking was undertaken to elucidate the mechanism of binding of the ligands as well as to identify small molecules with high cooperativity [75] and affinity to the *Ld*SMT. An evaluation of the 2D interactions [42] showed that the compounds including 22,26-azasterol and the three drugs interacted with amino acid residues Asp25, Ala28, Phe93, Phe100, Trp208, Asp218, Arg227, Ile228, Ala311, Glu320, and Leu322, consistent with previous studies [29,76]. Specific interactions in all of the complexes included *pi*–anion, *pi*–*pi* stacking, *pi*–alkyl, *pi*–sigma, carbon–hydrogen, and hydrogen bonds.

STOCK6S-06707, STOCK6S-55084, and STOCK6S-14893 did not form hydrogen bonds with any of the amino acid residues in the binding site. On the contrary, hydrogen bond interactions were observed for STOCK6S-65920 and STOCK6S-16994 via Ser330 and Thr338 (Table 2 and Supplementary Figure S1a,b). STOCK6S-06707 (−8.7 kcal/mol) only formed hydrophobic interactions with Asp25, Ala28, Aso31, Arg32, Phe307, and Ala311 (Table 2 and Figure 5). In addition, STOCK6S-64941 and STOCK6S-19430 formed two hydrogen bonds with active site residues (Table 2, Supplementary Figure S1d,e), while STOCK6S-84928 and STOCK6S-07353 formed three hydrogen bonds. Hydrophobic interaction analysis showed that Leu13, Trp208, Ile224, Tyr316, Lys313, and Leu322 (Table 2, Figure 5, and Supplementary Figure S1g) could be essential for the ligand binding of STOCK6S-84928, STOCK6S-07353, STOCK6S-64941, and STOCK6S-19430. Furthermore, STOCK6S-16994, STOCK6S-55084, and STOCK6S-65920 formed hydrophobic interactions with Phe93, Ile228, Glu192, and Arg195 (Table 2, Supplementary Figure S1a,c), which could enhance the protein–ligand stability. This result corroborates earlier studies demonstrating that amino acids between the ranges 15–100, 200–250, and 280–320 were critical for ligand binding [28,29,77].

The known inhibitor 22,26-azasterol (−7.6 kcal/mol) formed hydrogen bonds with Glu102 and Gly200 (Table 2 and Supplementary Figure S1h). Then, paromomycin, amphotericin B, and miltefosine formed five, four, and one hydrogen bond(s), respectively. The hydrophobic interactions formed by 22,26-azasterol and known drugs with Phe100, Lys198, Pro199, and Glu306 (Table 2 and Supplementary Figure S1h–k) may support the stability of the complexes.

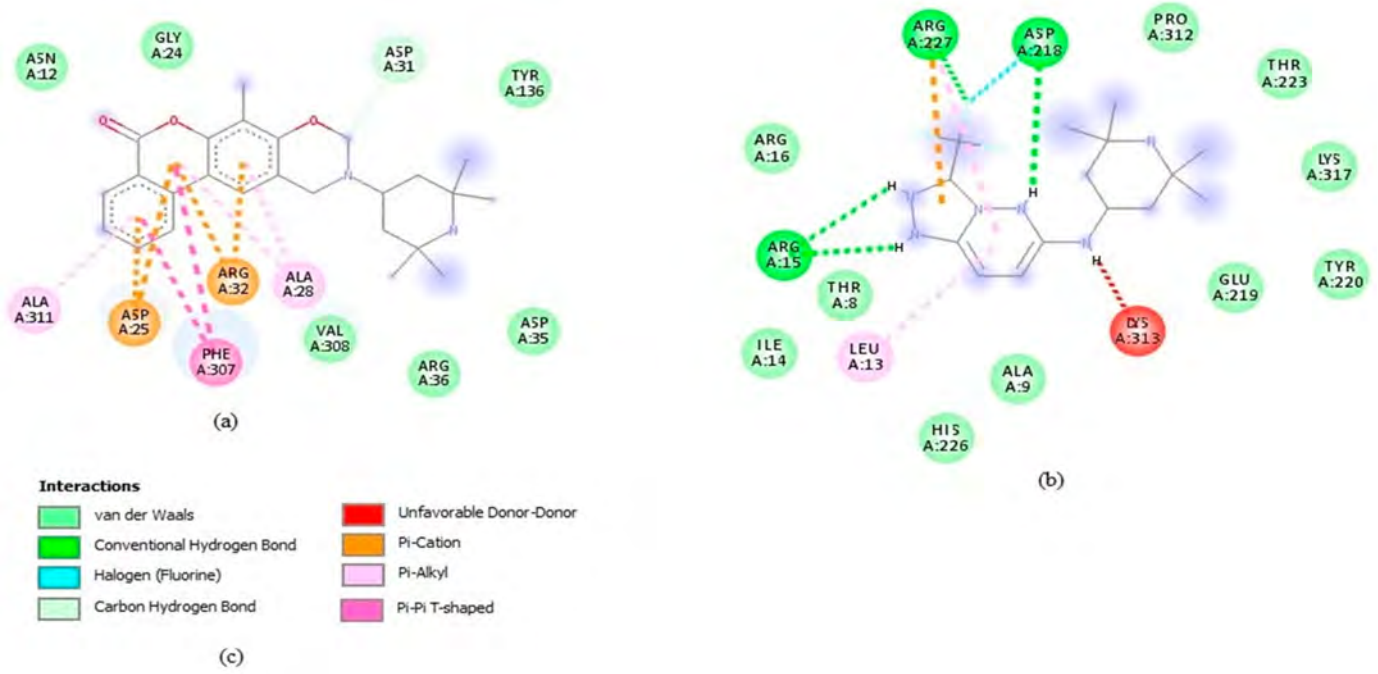

Figure 5. Two-dimensional interactions of the *Ld*SMT-hit complexes as visualised in Discovery Studio v.19.1.0.18287 [42]. (**a**) *Ld*SMT-STOCK6S-06707 complex, (**b**) *Ld*SMT-STOCK6S-84928 complex, and (**c**) legend of interactions.

3.8. ADMET Profiling

The drug-likeness of the nine selected compounds was evaluated using Lipinski's rule of five (Ro5) [78,79]. According to the Ro5, a compound is classified as drug-like and orally active if it conforms to the following criteria: a molecular weight ≤500 Da, an octanol–water partition coefficient log $p \leq 5$, HBD ≤ 5, and HBA ≤ 10 [79]. The Ro5 has been applied in many studies, especially during the shortlisting of hits [80–82]. The physicochemical properties and drug-likeness computed via SwissADME [50] showed that none of the compounds violated any of the Ro5 (Table 3). Orally active drugs, according to Veber's rule, must possess a maximum of 10 rotatable bonds as well as a polar surface area of less than 140 Å^2 [83]. All nine hits were predicted to have less than 10 and 140 Å^2 for the number of rotatable bonds and polar surface area, respectively. STOCK6S-64941 had the highest number of rotatable bonds (6) and a polar surface area of 80.57 Å^2. The results (Table 3) suggest that the selected compounds possess the potential to be orally active [83].

Molar refractivity (MR) measurement was conducted to assess the movement of the compounds through the body and their ability to reach their targets of inhibition at optimum concentrations [84]. MR for druggable candidates is recommended to be between 40 and 130 [29]. All of the selected compounds were found to possess MR within this range except STOCK6S-64941 with an MR of 130.16 (Table 3).

For drugs to be transported by the circulatory system to their site of activity, they are required to be soluble [85]. The computed solubility profile of the compounds showed them as soluble and hence possess the potential to reach their target sites at maximum concentrations (Table 3). Furthermore, the bioavailability score (BS), which measures the ability of drugs to reach systemic circulation, was also estimated [86]. The computed BS for the compounds was 0.55, similar to the reported studies (Table 3) [29,86].

Table 3. Predicted physicochemical and pharmacological properties of the selected hit compounds. Molecular weight (MW), number of rotatable bonds (NRB), molar refractivity (MR), topological polar surface area (TPSA), gastrointestinal absorption (GI), blood–brain barrier (BBB), number of Ro5 violations (vRoF), bioavailability score (BS), and solubility score (SC) are presented.

Compound ID	MW (g/mol)	NRB	MR	TPSA (Å^2)	LogS	SC	BS	GI	BBB	vRoF
STOCK6S-06707	406.52	1	129.05	54.71	−5.31	Moderate	0.55	High	Yes	0
STOCK6S-84928	342.36	3	88.22	67.14	−3.39	Soluble	0.55	High	Yes	0
STOCK6S-65920	353.39	2	103.42	42.68	−4.73	Moderate	0.55	High	Yes	0
STOCK6S-55084	407.36	3	103.46	42.68	−5.27	Moderate	0.55	High	No	0
STOCK6S-64941	434.53	6	130.16	80.57	−5.62	Moderate	0.55	High	No	0
STOCK6S-19430	428.52	4	127.41	81.01	−4.01	Moderate	0.55	High	No	0
STOCK6S-14893	410.55	1	128.98	54.71	−5.11	Moderate	0.55	High	Yes	0
STOCK6S-07353	282.31	5	78.96	38.06	−3.03	Soluble	0.55	High	Yes	0
STOCK6S-16994	384.51	2	121.32	54.71	−4.5	Soluble	0.55	High	Yes	0
22,26-Azasterol	403.64	2	125.08	52.49	−5.66	Moderate	0.55	High	Yes	1
Amphotericin B	924.08	3	239.06	319.61	−5.37	Moderate	0.55	Low	No	3
Miltefosine	407.57	20	115.9	68.40	−5.32	Moderate	0.55	Low	No	0
Paromomycin	615.63	9	133.56	347.32	−2.44	Soluble	0.55	Low	No	3

The ability of a drug to cross the blood–brain barrier (BBB) to the brain is called BBB permeation [87]. Drugs with the ability to cross the BBB could bind to certain receptors to elicit the required pharmacological activities within the brain parenchyma. STOCK6S-55084, STOCK6S-64941, and STOCK6S-19430 (Table 3) were predicted not to be BBB permeants. Previous reports showed that *Leishmania* parasites infect and inflame the central nervous system (CNS) [88–90] and drugs with the potential of crossing the BBB could mediate in the elimination of the parasites in the CNS.

Next, we investigated the gastrointestinal absorption of the compounds. Together with 22,26-azatserol, they were predicted to possess high gastrointestinal absorption, suggesting a high probability of absorption into the bloodstream. On the contrary, the three drugs, amphotericin B, miltefosine, and paromomycin, were predicted to show low gastrointestinal absorption (Table 3). A previous study to identify potential inhibitors of *L. donovani* cell division cycle-2-related kinase 12 (CRK12) predicted compounds to possess high gastrointestinal absorption [32].

Furthermore, the toxicity profile (Table 4) of the compounds was evaluated using OSIRIS DataWarrior 5.0.0 [51]. The results showed that all of them were predicted not to be mutagenic or tumorigenic. On the other hand, STOCK6S-0670 was predicted as a high irritant, whilst STOCK6S-65920 and STOCK6S-55084 were found to possess low reproductive effects. Compounds STOCK6S-19430, STOCK6S-14893, and STOCK6S-16994 were predicted to possess high irritant and reproductive effects (Table 4).

3.9. Biological Activity Predictions of Selected Hit Compounds

The biological activities of the selected compounds were predicted [52] based on the structure–activity relationship. Compounds predicted with a probability of activity (Pa) greater than the probability of inactivity (Pi) have high chances of exhibiting the expected biological activities, hence could be considered for experimental validation [52,81].

All nine selected compounds were predicted to possess antineoplastic properties with Pa greater Pi, whilst STOCK6S-65920 and STOCK6S-55084 also act as CDK9 inhibitors (Supplementary Table S1). The anticancer drugs sunitinib, sorafenib, and lapatinib, which are known CDK inhibitors, were predicted as antileishmanial [30–32].

Table 4. Toxicity profiles of the selected compounds predicted using OSIRIS DataWarrior 5.0.0.

Ligand	DataWarrior Predictions			
	Tumorigenic	**Mutagenic**	**Irritant**	**Reproductive Effect**
STOCK6S-06707	None	None	High	None
STOCK6S-84928	None	None	None	None
STOCK6S-65920	None	None	None	Low
STOCK6S-55084	None	None	None	Low
STOCK6S-64941	None	None	None	High
STOCK6S-19430	None	None	High	high
STOCK6S-14893	None	None	High	High
STOCK6S-07353	None	None	None	None
STOCK6S-16994	None	None	High	High
22,26-Azasterol	None	None	None	None
Amphotericin B	None	None	None	None
Miltefosine	None	None	None	None
Paromomycin	None	None	None	None

Furthermore, four of the selected hit compounds, STOCK6S-06707, STOCK6S-84928, STOCK6S-14893, and STOCK6S-16994, were predicted (Supplementary Table S1) to be dermatologic, suggesting that they could be developed as a potential treatment for post-kala-azar leishmaniasis [91,92]. The compounds STOCK6S-65920 and STOCK6S-55084 were also predicted to be inhibitors of lanosterol 14alpha demethylase. The drugs ketoconazole, fluconazole, itraconazole, and posaconazole are already in various clinical stages for leishmaniasis treatment targeting the *Leishmania* parasites lanosterol 14alpha demethylase [93,94].

STOCK6S-64941 and STOCK6S-07353 were predicted as potential aspulvinone dimethylallyl transferase and indole pyruvate C-methyltransferase inhibitors (Supplementary Table S1), respectively. The *Ld*SMT belongs to the family of methyltransferases to which aspulvinone dimethylallyl transferase and indole pyruvate C-methyltransferase also belong [95–97]. The predicted inhibition of these two targets suggests the potential of the selected hit compounds to suppress *L. donovani* sterol methyltransferase.

Furthermore, five of the selected hits comprising STOCK6S-06707, STOCK6S-55084, STOCK6S-19430, STOCK6S-14893, and STOCK6S-16994 were predicted for Alzheimer's treatment (Supplementary Table S1) with Pa greater than Pi. A recent in vitro study identified perphenazine, a known drug for Alzheimer's treatment, to possess antileishmanial potential with EC_{50} of 1.2 μg/mL [98]. Similarly, clomipramine, a drug for Alzheimer's treatments, induced programmed cell death in *L. amazonensis* via a mitochondrial pathway disruption with an IC_{50} of 8.31 μM [99,100]. The predicted biological activities and mechanisms suggest that the selected compounds have potential antileishmanial scaffolds.

3.10. MD Simulations Analyses

Three of the hit compounds, STOCK6S-06707, STOCK6S-84928, and STOCK6S-65920, were selected for downstream MD simulation analysis. They possessed low binding energies, reasonable pharmacological profiles, and desirable biological activities. The control used for the MD was 22,26-azasterol. A 100 ns MD simulation was performed to assess the structural stability and the conformational dynamics of the *Ld*SMT–analogue complexes. The RMSDs were computed to ascertain the stability of the protein–ligand complexes (Supplementary Figure S2). The complexes showed comparable stability to the unbound protein and protein–22,26-azasterol complex. The unbound *Ld*SMT and the protein–ligand complexes experienced a high volatility within the first 10 ns of the MD simulation with an RMSD fluctuation of 0.15 nm (Supplementary Figure S2a), which is classified as acceptable, since the drifting falls within the range 0.1–0.3 ns [101]. Equilibration was therefore reached afterward with a low RMSD fluctuation of $\leq$0.05nm. Remarkably, the RMSD results produced were corroborated by the RMSF values (Supplementary Figure S3a).

The probability distribution function (PDF) analysis revealed that all of the complexes, including the unbound protein, had only one peak, meaning the complexes and the unbound protein were stable with fewer deviations. This corroborates SARS-CoV-2 main protease (M^{pro}) studies using malaria box compounds as hits [102] and the screening of inhibitors against *Leishmania donovani* 3-mercapto pyruvate sulfurtransferase [103]. The unbound protein, 22,26-azasterol, STOCK6S-84928, and STOCK6S-65920 complexes reached equilibrium with an average RMSD of 0.25 nm (Supplementary Figure S2a,b). In addition, the average RMSDs for the *Ld*SMT–STOCK6S-06707, *Ld*SMT–STOCK6S-84928, *Ld*SMT–STOCK6S-65920, *Ld*SMT–22,26-azasterol, and *Ld*SMT were 0.25 ± 0.03, 0.25 ± 0.03, 0.25 ± 0.02, 0.25 ± 0.03, and 0.25 ± 0.02, respectively, and were lower compared to an earlier study [29]. Overall, the compounds maintained a stable pose within the binding pocket of *Ld*SMT compared to the 22,26-azasterol.

The contributions of the amino acid residues to the stability of the protein–ligand complexes were analysed by computing RMSFs [104] (Supplementary Figure S3a). Despite the differences in the RMSFs, the fluctuation trends are similar among all of the complexes. The maximum fluctuations occurred for amino acid residues between 10–90, 100–160, 200–250, and 280–320 (Supplementary Figure S3a), and hence could be considered critical for ligand binding. Notably, from the PDF analysis (Supplementary Figure S3b) of the RMSF trajectory, the three hit compounds, *Ld*SMT–STOCK6S-06707, *Ld*SMT–STOCK6S-84928, *Ld*SMT–STOCK6S-65920, had average RMSFs of 0.13 ± 0.04, 0.15 ± 0.04, and 0.15 ± 0.04, respectively, compared to *Ld*SMT–22,26-azasterol (0.10 ± 0.04). Moreover, the unbound *Ld*SMT also had a similar average RMSF of 0.15 ± 0.04. Contrasting the RMSD and RMSF plots, the complexes were observed to be stable and comparable to the *Ld*SMT–22,26-azasterol complex.

The rigidness of the unbound protein and the complexes for the entire simulation period is determined by Rg [32]. A folded protein normally maintains a relatively steady Rg over a given simulation period when compared to the unfolded period. The computed Rg plot showed that the complexes maintained steady stability over the entire period with the *Ld*SMT–STOCK65-06707 and *Ld*SMT–STOCK6S-84928 showing the lowest average Rg of 1.975 ± 0.02 and 1.975 ± 0.01 nm, respectively (Supplementary Figure S4a). Similarly, 22,26-azasterol, STOCK6S-65920 complexes, and the unbound *Ld*SMT recorded respective averages of Rg of about 2.0 ± 0.01, 1.975 ± 0.03, and 2.0 ± 0.01 nm, respectively. As per the PDF analysis, all of the complexes and the native protein had only one peak. Both the unbound *Ld*SMT and *Ld*SMT–ligand complexes had an average Rg of 2 nm (Supplementary Figure S4b). Furthermore, the Rg graph (Figure 6) indicates that the compactness of the *Ld*SMT–STOCK6S-06707, *Ld*SMT–STOCK6S-84928, and *Ld*SMT–STOCK6S-65920 was maintained and kept steady after complex formation.

To determine the effect of loose packing on solvent accessibility, the SASA of the entire protein was computed to provide information on the protein–solvent interactions [103,105]. Generally, high SASA values imply an increase in structural enlargement for the protein–ligand complexes under the influence of solvent surface charges, resulting in a more flexible and unstable conformation [105]. A complex of *L. donovani* 3-mercapto pyruvate sulfurtransferase and rutin complex had an average SASA value of 44 nm^2, which was more compact than the unbound protein with an average SASA of 48 nm^2 [103]. In the current study, no differences were observed (Supplementary Figure S5a) for the unbound protein, the three hits, and 22,26-azasterol complexes. The computed average SASA value for the unbound *Ld*SMT, 22,26-azasterol, and the identified lead complex were 160 nm^2 (Supplementary Figure S5a). In addition, per the PDF SASA analysis, the unbound *Ld*SMT, as well as 22,26-azasterol, STOCK6S-06707, STOCK6S-84928, and STOCK6S-65920 complexes, had average SASA values of 155.0 ± 5.4, 160.0 ± 5.3, 158.0 ± 6.1, 160.0 ± 4.8, and 155 ± 6.4 nm^2 (Supplementary Figure S5b), respectively. The hit compounds formed stable hydrophobic interactions with *Ld*SMT compared to that of 22,26-azasterol.

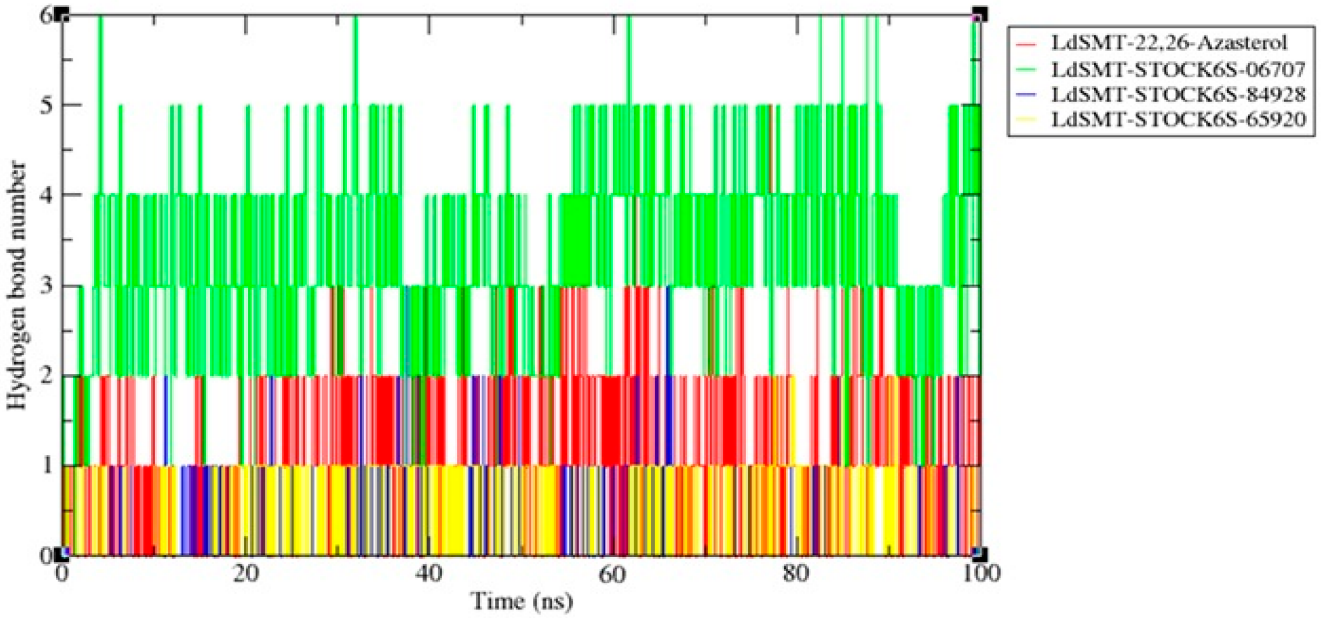

Figure 6. Number of hydrogen bond interactions of the protein–ligand complexes throughout the MD simulation period. Number of hydrogen bonds in *Ld*SMT–22,26-azasterol, *Ld*SMT–STOCK6S-06707, *Ld*SMT–STOCK6S-84928, and *Ld*SMT–STOCK6S-65920 complexes.

To better understand the binding interactions that influenced the binding energy of the various protein–ligand complexes, the MD simulation was carried out to calculate the number of HB formed for all the *Ld*SMT–analogue complexes. The number of HB formed were (6 ± 1), (5 ± 1), (3 ± 1), and (2 ± 1) (Figure 6) for the *Ld*SMT–STOCK6S-06707, *Ld*SMT–22,26-azasterol, *Ld*SMT–STOCK6S-84928, and *Ld*SMT–STOCK6S-65920 complexes, respectively. Altogether, the hydrogen and hydrophobic interactions showed strong binding of the hit compounds in the active site of the *Ld*SMT.

3.11. MM/PBSA Computation of Free Binding Energies

Comparatively, binding free energy calculations from simulation studies have been proven to be more accurate than their docking counterparts and can prioritise compounds more efficiently for experimental evaluation [106]. Therefore, this work further employed MM/PBSA in computing the binding free energies of the protein–ligand complexes. Notably, a high negative binding free energy of a complex signifies a strong affinity of the ligand to the target protein. Among the selected hit compounds, STOCK6S-06707 with the lowest binding energy of −8.7 kcal/mol from the docking studies also recorded the lowest binding free energy of -371.146 ± 2.105 kJ/mol (Table 5). While STOCK6S-84928 and STOCK6S-65920 showed binding free energies of -129.725 ± 4.799 and -149.899 ± 3.6 kJ/mol, respectively, their binding free energies were higher than 22,26-azasterol (-221.527 ± 3.716 kJ/mol). The lead compounds showed promising binding free energies comparable to 22,26-azasterol and therefore warrant experimental validation. The free binding energy was contributed by van der Waal (ΔG_{vdW}), electrostatic (ΔG_{ele}), polar solvation ($\Delta G_{pol,\,sol}$), and SASA (ΔG_{SASA}). Among these energies, van der Waal, responsible for the embedded hydrophobic interactions between the residues in the binding pocket and lead compounds, was the major contributor to the binding free energy (Table 5), followed by electrostatic. The results presented in this work corroborate previous studies that have shown that both van der Waal and electrostatic energies were responsible for the stability of protein–ligand complexes [29,32]. Despite the role of entropy in computing the free energy of binding to protein–ligand complexes [107], the current study did not take into account this contribution, because entropy tends to produce negligible effects when

comparing the binding strength of ligands inhibiting the same protein target [108] and could be computationally expensive.

Table 5. Contributions of van der Waal, electrostatic, polar solvation, and solvent-accessible surface area energies to the binding free energy of the protein–ligand complexes.

Complex	ΔG_{vdW} (kJ/mol)	ΔG_{ele} (kJ/mol)	$\Delta G_{pol,sol}$ (kJ/mol)	ΔG_{SASA} (kJ/mol)	ΔG_{bind} (kJ/mol)
STOCKIN6S-O6707	−232.978 ± 1.954	−983.173 ± 4.875	863.728 ± 3.447	−18.722 ± 2.602	−371.146 ± 2.105
STOCKIN6S−84928	−142.275 ± 5.679	−3.390 ± 0.417	29.163 ± 2.101	−13.223 ± 4.385	−129.725 ± 4.799
STOCKIN6S-65920	−217.243 ± 3.589	−6.439 ± 1.576	90.570 ± 4.465	−16.786 ± 1.646	−149.899 ± 3.600
22,26-Azasterol	−186.874 ± 2.143	−217.654 ± 0.546	199.212 ± 4.701	−16.211 ± 1.632	−221.527 ± 3.716

Favourable interactions between the binding site residues of the target protein and ligand result in the stability of the complex, and this was assessed by the per-residue decomposition, which computes the energy contribution of each of the amino acids. Generally, amino acids that contribute energies greater than +5 kJ/mol or lower than −5 kJ/mol are regarded as critical for ligand binding [59]. From the docking studies, residues Asp25, Ala28, Phe93, Phe100, Trp208, Asp218, Arg227, Ile228, Ala311, Glu320, and Leu322 were found to be key for ligand binding. The MM/PBSA per-residue decomposition computations revealed that Asp25 and Trp208 (Figure 7) contributed energies of −20 and −48 kJ/mol, respectively, for the stability of the *Ld*SMT–STOCK6S-06707 complex. Furthermore, the amino acid Trp208 contributed an energy of −10 kJ/mol () for the stability of STOCK6S-65920. The 22,26-azasterol complex generated per-residue decomposition trajectory with Glu102, Phe194, Phe198, and Gly200 (Supplementary Figure S6b,c), contributing energies above and below the threshold critical for ligand binding. Similarly, the per-residue decomposition trajectory of the STOCK6S-84928 complex shows Trp208 to produce energy of −7 kJ/mol for ligand binding. An earlier study to identify the potential inhibitors of *Ld*SMT showed similar residues as being critical for ligand binding [29]. The amino acid residues within the binding pocket, including Asp25 and Trp208 of *Ld*SMT, contributed meaningful energies to the stability of the complexes.

3.12. In Vitro Evaluation of Identified Hits against Leishmania donovani

The antileishmanial properties of three purchasable hit compounds, STOCK6S-06707, STOCK6S-84928, and STOCK6S-65920, were tested in vitro. The effects of different concentrations (Supplementary Figure S7) on the survival of *L. donovani* promastigotes were studied with amphotericin B treatment as a positive control (Table 6). After 72 h of treatments of *L. donovani* promastigote cultures with varying concentrations of the three compounds, effect-based dose finding analysis revealed that concentrations of 21.9 ± 1.5 µM, 23.5 ± 1.1 µM, and 118.3 ± 5.8 µM (Table 6) for STOCK6S-06707, STOCK6S-65920, and STOCK6S-84928, respectively, eliminated 50 % of *L. donovani* promastigotes. Amphotericin B exhibited IC_{50} of 6.56 ± 0.06 µM. Despite the significant inhibitory effects of the hit compounds, their potencies were lower compared to amphotericin B. This notwithstanding, the compounds can be optimised to improve potency.

Both *Leishmania* and *Trypanosoma spp*. belong to the family of kinetoplastids [109] and some compounds have been shown to inhibit the survival of both *Leishmania* parasites and *Trypanosoma spp.* [110–112]. Compound SQ10, which suppressed the growth of *L. donovani*, was also reported to possess activity against *T. cruzi* [112]. Moreover, 22,26-azasterol, which inhibits sterol methyltransferase, also inhibits *T. cruzi* and *T. brucei* [25]. The anti-trypanosomal effects of the three compounds against *T. brucei* with diminazene as a positive control (Table 6) were undertaken via in vitro testing. Two of the compounds showed anti-trypanosomal activity with IC_{50} values of 14.3 ± 2.0 µM (STOCK6S-84928) and 18.1 ± 1.4 µM (STOCK6S-65920). Despite the lower activity of the two compounds

compared to diminazene, they still possess significant inhibitory effects against *T. cruzi* and are hence worthy of further studies.

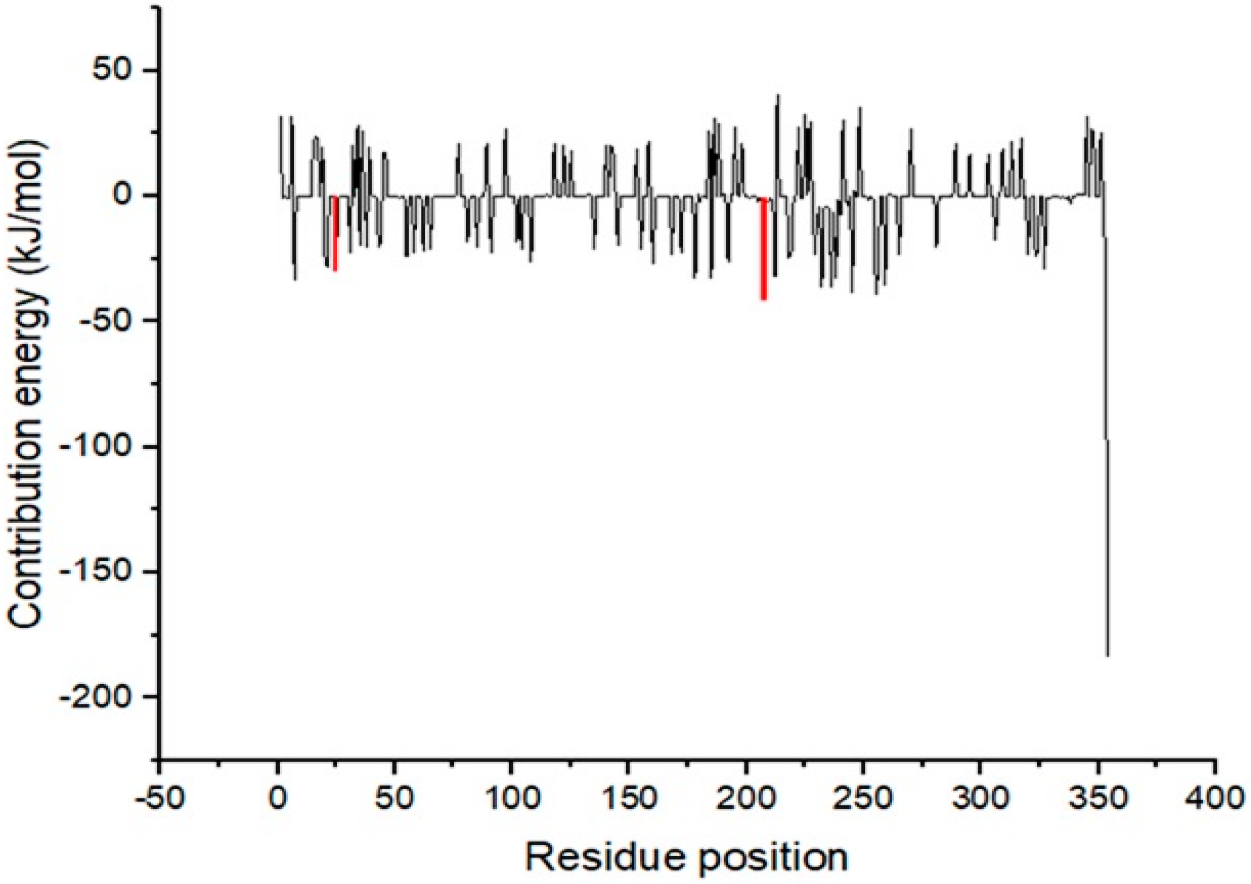

Figure 7. MM/PBSA computation of per-residue energy decomposition for the *Ld*SMT-STOCK6S-06707 complex.

Table 6. Results from the in vitro studies of the selected hit compounds against the promastigotes of *Leishmania donovani* and *Trypanosoma brucei*.

Compound	*Leishmania donovani* IC_{50} (μM) ± SD	*Trypanosoma brucei* (IC_{50}) (μM) ± SD
STOCK6S-65920	23.5 ± 1.1	18.1 ± 1.4
STOCK6S-06707	21.9 ± 1.5	NA
STOCK6S-84928	118.3 ± 5.8	14.3 ± 2.0
Amphotericin B	6.56 ± 0.06	-
Diminazene	-	0.1 ± 0.02

NA = not available.

4. Contribution to the Field

In addition to the limited number, the available chemotherapeutic agents for the treatment of visceral leishmaniasis are plagued with inefficiencies and chemoresistance [113]. The integrated *In silico* and in vitro study, therefore, augments the current efforts in discovering antileishmanial agents by identifying inhibitors with the potential to circumvent the activities of *Leishmania donovani*. The elucidation of the mechanisms of binding of the potential lead compounds provides the platform for the identification of other potent inhibitors for leishmaniasis treatment targeting sterol methyltransferase.

5. Conclusions

Sterol methyltransferase is expressed in all *Leishmania* parasites, but does not have human homologues, making it a potential target for drug design against leishmaniasis. This study used *In silico* techniques including pharmacophore-based virtual screening, molecular docking, and MD simulations, as well as in vitro approaches to identify potent inhibitors against *Ld*SMT. Three compounds, STOCK6S-06707, STOCK6S-84928, and STOCK6S-65920, had a high binding affinity with binding energies lower than those of known inhibitors including 22,26-azasterol (−7.6 kcal/mol) and the antileishmanial drugs amphotericin B (−5.3 kcal/mol), miltefosine (−5.0 kcal/mol), and paromomycin (−4.0 kcal/mol). Molecular dynamics simulations and mechanistic studies revealed the leads to interact with critical amino acids in the binding site in the attenuation of *Ld*SMT. The compounds were predicted as antileishmanial with acceptable pharmacological and toxicity profiles. STOCK6S-06707, STOCK6S-84928, and STOCK6S-65920 were shown to suppress promastigotes of *L. donovani* cultures with IC_{50} values of 21.9, 23.5, and 118.3 µM, respectively. When the hits were tested for their anti-trypanosomal activity against *T. brucei*, STOCK6S-84928 and STOCK6S-65920 were active with IC_{50} of 14.3 and 18.1 µM, respectively. The promising antileishmanial compounds identified could serve as a basis for the design of potent biotherapeutic moieties.

Supplementary Materials: The following supporting information can be downloaded at: https://www.mdpi.com/article/10.3390/ph16030330/s1, Figure S1. The cartoon representations and 2D interactions of the *Ld*SMT-hits complexes as visualized in Discovery Studio v19.1.0.18287. (a) Complexes of *Ld*SMT-STOCK6S-65920, (b) *Ld*SMT-STOCK6S-16994, (c) *Ld*SMT-STOCK6S-55084, (d) *Ld*SMT-STOCK6S-64941, (e) *Ld*SMT-STOCK6S-19430, (f) *Ld*SMT-STOCK6S-14893, (g) *Ld*SMT-STOCK6S-07353, (h) *Ld*SMT-azasterol, (i) *Ld*SMT-paromomycin, (j) *Ld*SMT-miltefosine, and (k) *Ld*SMT-amphotericin B. Figure S2. The RMSD andPDF analysis of 100 ns trajectory of the unbound *Ld*SMT, complexes of the three selected hits and azasterol. (a) RMSD for unbound protein and all the complexes, (b) PDF of RMSD unbound *Ld*SMT, *Ld*SMT-22,26-Azasterol, *Ld*SMT-STOCK6S-06707, *Ld*SMT-STOCK6S-84928 and *Ld*SMT-STOCK6S-65920). Figure S3. (a) Combined RMSF plot for the unbound *Ld*SMT and the protein-ligand complexes and (b) PDF of RMSF unbound *Ld*SMT, *Ld*SMT-22,26-Azasterol, *Ld*SMT-STOCK6S-06707, *Ld*SMT-STOCK6S-84928 and *Ld*SMT-STOCK6S-65920), Figure S4. Rg analysis of 100 ns trajectory of the unbound *Ld*SMT, complexes of the three selected hits and 22,26-azasterol complex. (a) Rg for unbound protein and all the complexes, (b) PDF of Rg of *Ld*SMT, *Ld*SMT-Azasterol, *Ld*SMT-STOCK6S-06707, *Ld*SMT-STOCK6S-84928 and *Ld*SMT-STOCK6S-65920). Figure S5. SASA analysis of 100 ns trajectory of the unbound *Ld*SMT, complexes of the three selected hits and azasterol complex. (a) SASA for unbound protein and all the complexes, (b) PDF of SASA for unbound *Ld*SMT, *Ld*SMT-22,26-azasterol, *Ld*SMT-STOCK6S-06707, *Ld*SMT-STOCK6S-84928 and *Ld*SMT-STOCK6S-65920. Figure S6. MMPBSA computes per-residue energy decomposition for the *Ld*SMT-STOCK6S-84928, *Ld*SMT-STOCK6S-65920 and *Ld*SMT-22,26-Azasterol complexes. Figure S7. Graphical representation of the *in vitro* activity of hit compounds targeting. (A) *Leishmania donovani* and (B) *Trypanosoma brucei*. (a) STOCK6S-06707, (b) STOCK6S-65920 and (c) STOCK6S-84928. Data represent the mean of three independent biological replicates. Table S1. Biological activity predictions of selected hit compounds with their probability of activity (Pa) and probability of inactivity (Pi).

Author Contributions: P.O.S., S.K.K. and R.K.A. conceptualised the project idea. P.O.S. designed the project and predominantly undertook all the computational analysis with inputs from S.K.K., R.K.A., E.B., W.A.M.III, and M.D.W., T.M.G. and J.K.T. provided the cells and supported the in vitro studies. P.O.S. wrote the first draft of the manuscript. All authors have read and agreed to the published version of the manuscript.

Funding: This research received no external funding.

Institutional Review Board Statement: Not applicable.

Informed Consent Statement: Not applicable.

Data Availability Statement: Not applicable.

Acknowledgments: The authors would like to show appreciation to Ghana National Petroleum Corporation (GNPC) for the scholarship awarded to Patrick Opare Sakyi for his postgraduate studies. We also acknowledge the West African Centre for Cell Biology of Infectious Pathogens (WACCBIP), and the University of Ghana for providing Zuputo, a DELL high-performance computing system. We appreciate the kind gesture of Yamthe Lauve for graciously providing the *Leishmania donovani* strain used in the in vitro studies.

Conflicts of Interest: The authors declare no conflict of interest regarding the manuscript and its contents.

References

1. Camargo, L.B.; Langoni, H. Impact of Leishmaniasis on Public Health. *J. Venom. Anim. Toxins incl. Trop. Dis.* **2006**, *12*, 527–548. [CrossRef]
2. Bamorovat, M.; Sharifi, I.; Tavakoli Oliaee, R.; Jafarzadeh, A.; Khosravi, A. Determinants of Unresponsiveness to Treatment in Cutaneous Leishmaniasis: A Focus on Anthroponotic Form Due to Leishmania Tropica. *Front. Microbiol.* **2021**, *12*, 1143–1158. [CrossRef]
3. Leta, S.; Dao, T.H.T.; Mesele, F.; Alemayehu, G. Visceral Leishmaniasis in Ethiopia: An Evolving Disease. *PLoS Negl. Trop. Dis.* **2014**, *8*, e3131. [CrossRef]
4. Simoben, C.V.; Ntie-Kang, F.; Akone, S.H.; Sippl, W. Compounds from African Medicinal Plants with Activities Against Selected Parasitic Diseases: Schistosomiasis, Trypanosomiasis, and Leishmaniasis. *Nat. Prod. Bioprospect.* **2018**, *8*, 151–169. [CrossRef]
5. Kwofie, S.K.; Broni, E.; Dankwa, B.; Enninful, K.S.; Kwarko, G.B.; Darko, L.; Durvasula, R.; Kempaiah, P.; Rathi, B.; Miller, W.A., III; et al. Outwitting an Old Neglected Nemesis: A Review on Leveraging Integrated Data-Driven Approaches to Aid in Unraveling of Leishmanicides of Therapeutic Potential. *Curr. Top. Med. Chem.* **2020**, *20*, 349–366. [CrossRef]
6. Tiwari, N.; Gedda, M.R.; Tiwari, V.K.; Singh, S.P.; Singh, R.K. Limitations of Current Therapeutic Options, Possible Drug Targets and Scope of Natural Products in Control of Leishmaniasis. *Mini-Rev. Med. Chem.* **2018**, *18*, 26–41. [CrossRef]
7. Singh, O.P.; Singh, B.; Chakravarty, J.; Sundar, S. Current Challenges in Treatment Options for Visceral Leishmaniasis in India: A Public Health Perspective. *Infect. Dis. Poverty* **2016**, *5*, 19. [CrossRef]
8. Sakyi, P.O.; Amewu, R.K.; Devine, R.N.O.A.; Ismaila, E.; Miller, W.A.; Kwofie, S.K. The Search for Putative Hits in Combating Leishmaniasis: The Contributions of Natural Products Over the Last Decade. *Nat. Prod. Bioprospect.* **2021**, *11*, 489–544. [CrossRef]
9. Singh, N.; Mishra, B.B.; Bajpai, S.; Singh, R.K.; Tiwari, V.K. Natural Product Based Leads to Fight against Leishmaniasis. *Bioorganic Med. Chem.* **2014**, *22*, 18–45. [CrossRef]
10. Ball, P. Chemistry: Why Synthesize? *Nature* **2015**, *528*, 327–329. [CrossRef]
11. Molinski, T.F.; Dalisay, D.S.; Lievens, S.L.; Saludes, J.P. Drug Development from Marine Natural Products. *Nat. Rev. Drug Discov.* **2009**, *8*, 69–85. [CrossRef]
12. Berdigaliyev, N.; Aljofan, M. An Overview of Drug Discovery and Development. *Future Med. Chem.* **2020**, *12*, 939–947. [CrossRef]
13. Osorio, Y.; Travi, B.L.; Renslo, A.R.; Peniche, A.G.; Melby, P.C. Identification of Small Molecule Lead Compounds for Visceral Leishmaniasis Using a Novel Ex Vivo Splenic Explant Model System. *PLoS Negl. Trop. Dis.* **2011**, *5*, e962. [CrossRef]
14. Zhang, M.Q.; Wilkinson, B. Drug Discovery beyond the 'Rule-of-Five'. *Curr. Opin. Biotechnol.* **2007**, *18*, 478–488. [CrossRef]
15. de la Torre, B.G.; Albericio, F. The Pharmaceutical Industry in 2021. An Analysis of FDA Drug Approvals from the Perspective of Molecules. *Molecules* **2022**, *27*, 1075. [CrossRef]
16. Beck, H.; Härter, M.; Haß, B.; Schmeck, C.; Baerfacker, L. Small Molecules and Their Impact in Drug Discovery: A Perspective on the Occasion of the 125th Anniversary of the Bayer Chemical Research Laboratory. *Drug Discov. Today* **2022**, *27*, 1560–1574. [CrossRef]
17. Chawla, B.; Madhubala, R. Drug Targets in Leishmania. *J. Parasit. Dis.* **2010**, *34*, 1–13. [CrossRef]
18. Jones, N.G.; Catta-Preta, C.M.C.; Lima, A.P.C.A.; Mottram, J.C. Genetically Validated Drug Targets in Leishmania: Current Knowledge and Future Prospects. *ACS Infect. Dis.* **2018**, *4*, 467–477. [CrossRef]
19. Le Pape, P. Development of New Antileishmanial Drugs—Current Knowledge and Future Prospects. *J. Enzym. Inhib. Med. Chem.* **2008**, *23*, 708–718. [CrossRef]
20. Mazire, P.; Agarwal, V.; Roy, A. Road-Map of Pre-Clinical Treatment for Visceral Leishmaniasis. *Drug Dev. Res.* **2022**, *83*, 317–327. [CrossRef]
21. Alcazar-Fuoli, L.; Mellado, E. Ergosterol Biosynthesis in Aspergillus Fumigatus: Its Relevance as an Antifungal Target and Role in Antifungal Drug Resistance. *Front. Microbiol.* **2012**, *3*, 439–445. [CrossRef]
22. Mukherjee, S.; Xu, W.; Hsu, F.F.; Patel, J.; Huang, J.; Zhang, K. Sterol Methyltransferase Is Required for Optimal Mitochondrial Function and Virulence in Leishmania Major. *Mol. Microbiol.* **2019**, *111*, 65–81. [CrossRef]
23. Rudmann, D.G. On-Target, and off-Target-Based Toxicologic Effects. *Toxicol. Pathol.* **2013**, *41*, 310–314. [CrossRef]
24. Kidane, M.E.; Vanderloop, B.H.; Zhou, W.; Thomas, C.D.; Ramos, E.; Singha, U.; Chaudhuri, M.; Nes, W.D. Sterol Methyltransferase a Target for Anti-Amoeba Therapy: Towards Transition State Analog and Suicide Substrate Drug Design. *J. Lipid Res.* **2017**, *58*, 2310–2323. [CrossRef]

25. Lorente, S.O.; Rodrigues, J.C.F.; Jiménez, C.J.; Joyce-Menekse, M.; Rodrigues, C.; Croft, S.L.; Yardley, V.; De Luca-Fradley, K.; Ruiz-Pérez, L.M.; Urbina, J.; et al. Novel Azasterols as Potential Agents for Treatment of Leishmaniasis and Trypanosomiasis. *Antimicrob. Agents Chemother.* **2004**, *48*, 2937–2950. [CrossRef]
26. Andrade-Neto, V.V.; Pereira, T.M.; do Canto-Cavalheiro, M.; Torres-Santos, E.C. Imipramine Alters the Sterol Profile in Leishmania Amazonensis and Increases Its Sensitivity to Miconazole. *Parasites Vectors* **2016**, *9*, 183. [CrossRef]
27. Torres-Santos, E.C.; Andrade-Neto, V.V.; Cunha-Júnior, E.F.; Do Canto-Cavalheiro, M.M.; Atella, G.C.; De Almeida Fernandes, T.; Costa, P.R.R. Antileishmanial Activity of Ezetimibe: Inhibition of Sterol Biosynthesis, in Vitro Synergy with Azoles, and Efficacy in Experimental Cutaneous Leishmaniasis. *Antimicrob. Agents Chemother.* **2016**, *60*, 6844–6852.
28. Tabrez, S.; Rahman, F.; Ali, R.; Muhammad, F.; Alshehri, B.M.; Alaidarous, M.A.; Banawas, S.; Dukhyil, A.A.B.; Rub, A. Repurposing of FDA-Approved Drugs as Inhibitors of Sterol C-24 Methyltransferase of Leishmania Donovani to Fight against Leishmaniasis. *Drug Dev. Res.* **2021**, *82*, 1154–1161. [CrossRef]
29. Sakyi, P.O.; Broni, E.; Amewu, R.K.; Miller, W.A.I.; Wilson, M.D.; Kwofie, S.K. Homology Modeling, de Novo Design of Ligands, and Molecular Docking Identify Potential Inhibitors of Leishmania Donovani 24-Sterol Methyltransferase. *Front. Cell. Infect. Microbiol.* **2022**, *12*, 859981. [CrossRef]
30. Perez, J.; Fuertes, M.; Nguewa, P.; Castilla, J.; Alonso, C. Anticancer Compounds as Leishmanicidal Drugs: Challenges in Chemotherapy and Future Perspectives. *Curr. Med. Chem.* **2008**, *15*, 433–439. [CrossRef]
31. Sanderson, L.; Yardley, V.; Croft, S.L. Activity of Anti-Cancer Protein Kinase Inhibitors against Leishmania spp. *J. Antimicrob. Chemother.* **2014**, *69*, 1888–1891. [CrossRef]
32. Broni, E.; Kwofie, S.K.; Asiedu, S.O.; Miller, W.A.; Wilson, M.D. A Molecular Modeling Approach to Identify Potential Antileishmanial Compounds Against the Cell Division Cycle (Cdc)-2-Related Kinase 12 (CRK12) Receptor of Leishmania Donovani. *Biomolecules* **2021**, *11*, 458. [CrossRef]
33. Kalmi, G.; Vignon-Pennamen, M.D.; Ram-Wolff, C.; Battistella, M.; Lafaurie, M.; Bouaziz, J.D.; Hamane, S.; Bernard, S.; Bretagne, S.; Thiéblemont, C.; et al. Visceral Leishmaniasis in Patients with Lymphoma: Case Reports and Review of the Literature. *Medicine* **2020**, *99*, e22787. [CrossRef]
34. Machado, P.R.L.; Ribeiro, C.S.; França-Costa, J.; Dourado, M.E.F.; Trinconi, C.T.; Yokoyama-Yasunaka, J.K.U.; Malta-Santos, H.; Borges, V.M.; Carvalho, E.M.; Uliana, S.R.B. Tamoxifen and Meglumine Antimoniate Combined Therapy in Cutaneous Leishmaniasis Patients: A Randomised Trial. *Trop. Med. Int. Health* **2018**, *23*, 936–942. [CrossRef]
35. Mak, K.K.; Pichika, M.R. Artificial Intelligence in Drug Development: Present Status and Future Prospects. *Drug Discov. Today* **2019**, *24*, 773–780. [CrossRef]
36. Pathania, S.; Singh, P.K.; Narang, R.K.; Rawal, R.K. Identifying Novel Putative ERK1/2 Inhibitors via Hybrid Scaffold Hopping –FBDD Approach. *J. Biomol. Struct. Dyn.* **2021**, *39*, 1–16. [CrossRef]
37. Wolber, G.; Langer, T. LigandScout: 3-D Pharmacophores Derived from Protein-Bound Ligands and Their Use as Virtual Screening Filters. *J. Chem. Inf. Model.* **2005**, *45*, 160–169. [CrossRef]
38. Eswar, N.; Eramian, D.; Webb, B.; Shen, M.Y.; Sali, A. Protein Structure Modeling with MODELLER. *Methods Mol. Biol.* **2008**, *426*, 145–159.
39. Siu, S.W.I.; Pluhackova, K.; Böckmann, R.A. Optimization of the OPLS-AA Force Field for Long Hydrocarbons. *J. Chem. Theory Comput.* **2012**, *8*, 1459–1470. [CrossRef]
40. Abraham, M.J.; Murtola, T.; Schulz, R.; Páll, S.; Smith, J.C.; Hess, B.; Lindahl, E. Gromacs: High-Performance Molecular Simulations through Multi-Level Parallelism from Laptops to Supercomputers. *Softwares* **2015**, *1*, 19–25. [CrossRef]
41. Van Der Spoel, D.; Lindahl, E.; Hess, B.; Groenhof, G.; Mark, A.E.; Berendsen, H.J.C. GROMACS: Fast, Flexible, and Free. *J. Comput. Chem.* **2005**, *26*, 1701–1718. [CrossRef]
42. Šudomová, M.; Hassan, S.T.S.; Khan, H.; Rasekhian, M.; Nabavi, S.M. A Multi-Biochemical and *In silico* Study on Anti-Enzymatic Actions of Pyroglutamic Acid against PDE-5, ACE, and Urease Using Various Analytical Techniques: Unexplored Pharmacological Properties and Cytotoxicity Evaluation. *Biomolecules* **2019**, *9*, 392. [CrossRef]
43. Trott, O.; Olson, A.J. AutoDock Vina: Improving the Speed and Accuracy of Docking with a New Scoring Function, Efficient Optimization, and Multithreading. *J. Comput. Chem.* **2010**, *31*, 455–461. [CrossRef]
44. Tian, W.; Chen, C.; Lei, X.; Zhao, J.; Liang, J. CASTp 3.0: Computed Atlas of Surface Topography of Proteins. *Nucleic Acids Res.* **2018**, *46*, W363–W367. [CrossRef]
45. Sorokina, M.; Steinbeck, C. Review on Natural Products Databases: Where to Find Data in 2020. *J. Cheminform.* **2020**, *12*, 20. [CrossRef]
46. Magaraci, F.; Jimenez, C.J.; Rodrigues, C.; Rodrigues, J.C.F.; Vianna Braga, M.; Yardley, V.; De Luca-Fradley, K.; Croft, S.L.; De Souza, W.; Ruiz-Perez, L.M.; et al. Azasterols as Inhibitors of Sterol 24-Methyltransferase in Leishmania Species and Trypanosoma Cruzi. *J. Med. Chem.* **2003**, *46*, 4714–4727. [CrossRef]
47. Mysinger, M.M.; Carchia, M.; Irwin, J.J.; Shoichet, B.K. Directory of Useful Decoys, Enhanced (DUD-E): Better Ligands and Decoys for Better Benchmarking. *J. Med. Chem.* **2012**, *55*, 6582–6594. [CrossRef]
48. Goksuluk, D.; Korkmaz, S.; Zararsiz, G.; Karaagaoglu, A.E. EasyROC: An Interactive Web Tool for ROC Curve Analysis Using R Language Environment. *R J.* **2016**, *8*, 213–230. [CrossRef]
49. Dallakyan, S.; Olson, A.J. Small-Molecule Library Screening by Docking with PyRx. *Methods Mol. Biol.* **2015**, *1263*, 243–250.

50. Daina, A.; Michielin, O.; Zoete, V. SwissADME: A Free Web Tool to Evaluate Pharmacokinetics, Drug-Likeness and Medicinal Chemistry Friendliness of Small Molecules. *Sci. Rep.* **2017**, *7*, 42717. [CrossRef]
51. Sander, T.; Freyss, J.; Von Korff, M.; Rufener, C. DataWarrior: An Open-Source Program For Chemistry Aware Data Visualization and Analysis. *J. Chem. Inf. Model.* **2015**, *55*, 460–473. [CrossRef]
52. Lagunin, A.; Stepanchikova, A.; Filimonov, D.; Poroikov, V. PASS: Prediction of Activity Spectra for Biologically Active Substances. *Bioinformatics* **2000**, *16*, 747–748. [CrossRef]
53. Jorgensen, W.L.; Tirado-Rives, J. Potential Energy Functions for Atomic-Level Simulations of Water and Organic and Biomolecular Systems. *Proc. Natl. Acad. Sci. USA* **2005**, *102*, 6665–6670. [CrossRef]
54. Lemkul, J.A. From Proteins to Perturbed Hamiltonians: A Suite of Tutorials for the GROMACS-2018 Molecular Simulation Package [Article v1.0]. *Living J. Comput. Mol. Sci.* **2019**, *1*, 5068. [CrossRef]
55. Dahiya, R.; Mohammad, T.; Gupta, P.; Haque, A.; Alajmi, M.F.; Hussain, A.; Hassan, M.I. Molecular Interaction Studies on Ellagic Acid for Its Anticancer Potential Targeting Pyruvate Dehydrogenase Kinase 3. *RSC Adv.* **2019**, *9*, 23302–23315. [CrossRef]
56. Kumari, R.; Kumar, R.; Lynn, A. G_mmpbsa —A GROMACS Tool for High-Throughput MM-PBSA Calculations. *J. Chem. Inf. Model.* **2014**, *54*, 1951–1962. [CrossRef]
57. Antwi, C.A.; Amisigo, C.M.; Adjimani, J.P.; Gwira, T.M. In Vitro Activity and Mode of Action of Phenolic Compounds on Leishmania Donovani. *PLoS Negl. Trop. Dis.* **2019**, *13*, e0007206. [CrossRef]
58. Amisigo, C.M.; Antwi, C.A.; Adjimani, J.P.; Gwira, T.M. In Vitro Anti-Trypanosomal Effects of Selected Phenolic Acids on Trypanosoma Brucei. *PLoS ONE* **2019**, *14*, e0216078. [CrossRef]
59. Kwofie, S.K.; Dolling, N.N.O.; Donkoh, E.; Laryea, G.M.; Mosi, L.; Miller, W.A.; Adinortey, M.B.; Wilson, M.D. Pharmacophore-Guided Identification of Natural Products as Potential Inhibitors of Mycobacterium Ulcerans Cystathionine γ-Synthase Metb. *Computation* **2021**, *9*, 32. [CrossRef]
60. Nahm, F.S. Receiver Operating Characteristic Curve: Overview and Practical Use for Clinicians. *Korean J. Anesthesiol.* **2022**, *75*, 25. [CrossRef]
61. Jung, S.W.; Kim, M.; Ramsey, S.; Kurtzman, T.; Cho, A.E. Water Pharmacophore: Designing Ligands Using Molecular Dynamics Simulations with Water. *Sci. Rep.* **2018**, *8*, 10400. [CrossRef]
62. Kchouk, S.; Hegazy, L. Pharmacophore Modeling for Biological Targets with High Flexibility: LXRβ Case Study. *Med. Drug Discov.* **2022**, *15*, 100135. [CrossRef]
63. Pascual, R.; Almansa, C.; Plata-Salamán, C.; Vela, J.M. A New Pharmacophore Model for the Design of Sigma-1 Ligands Validated on a Large Experimental Dataset. *Front. Pharmacol.* **2019**, *10*, 519. [CrossRef]
64. Verdonk, M.L.; Taylor, R.D.; Chessari, G.; Murray, C.W. Illustration of Current Challenges in Molecular Docking. In *Structure-Based Drug Discovery*; Springer: Dordrecht, The Netherlands, 2007.
65. Hsin, K.Y.; Matsuoka, Y.; Asai, Y.; Kamiyoshi, K.; Watanabe, T.; Kawaoka, Y.; Kitano, H. SystemsDock: A Web Server for Network Pharmacology-Based Prediction and Analysis. *Nucleic Acids Res.* **2016**, *44*, W507–W513. [CrossRef]
66. Mandrekar, J.N. Receiver Operating Characteristic Curve in Diagnostic Test Assessment. *J. Thorac. Oncol.* **2010**, *5*, 1315–1316. [CrossRef]
67. Kaserer, T.; Beck, K.R.; Akram, M.; Odermatt, A.; Schuster, D.; Willett, P. Pharmacophore Models, and Pharmacophore-Based Virtual Screening: Concepts and Applications Exemplified on Hydroxysteroid Dehydrogenases. *Molecules* **2015**, *20*, 22799–22832. [CrossRef]
68. Chen, Z.; Li, H.L.; Zhang, Q.J.; Bao, X.G.; Yu, K.Q.; Luo, X.M.; Zhu, W.L.; Jiang, H.L. Pharmacophore-Based Virtual Screening versus Docking-Based Virtual Screening: A Benchmark Comparison against Eight Targets. *Acta Pharmacol. Sin.* **2009**, *30*, 1694–1708. [CrossRef]
69. Sharma, V.; Panwar, A.; Gupta, G.K.; Sharma, A.K. Molecular Docking and MD: Mimicking the Real Biological Process. *Silico Chem. Biol. Curr. Futur. Prospect.* **2022**, *7*, 133–144. [CrossRef]
70. Sun, Z.; Zheng, L.; Wang, K.; Huai, Z.; Liu, Z. Primary vs Secondary: Directionalized Guest Coordination in β-Cyclodextrin Derivatives. *Carbohydr. Polym.* **2022**, *297*, 120050. [CrossRef]
71. Duan, L.L.; Feng, G.Q.; Zhang, Q.G. Large-Scale Molecular Dynamics Simulation: Effect of Polarization on Thrombin-Ligand Binding Energy. *Sci. Rep.* **2016**, *6*, 31488. [CrossRef]
72. Swegat, W.; Schlitter, J.; Krüger, P.; Wollmer, A. MD Simulation of Protein-Ligand Interaction: Formation and Dissociation of an Insulin-Phenol Complex. *Biophys. J.* **2003**, *84*, 1493. [CrossRef]
73. Mady, F.M.; Aly, U.F. Experimental, Molecular Docking Investigations and Bioavailability Study on the Inclusion Complexes of Finasteride and Cyclodextrins. *Drug Des. Devel. Ther.* **2017**, *11*, 1681. [CrossRef]
74. Gupta, Y.; Maciorowski, D.; Zak, S.E.; Jones, K.A.; Kathayat, R.S.; Azizi, S.A.; Mathur, R.; Pearce, C.M.; Ilc, D.J.; Husein, H.; et al. Bisindolylmaleimide IX: A Novel Anti-SARS-CoV-2 Agent Targeting Viral Main Protease 3CLpro Demonstrated by Virtual Screening Pipeline and in-Vitro Validation Assays. *Methods* **2021**, *195*, 57–71. [CrossRef]
75. Li, J.; McKay, K.T.; Remington, J.M.; Schneebeli, S.T. A Computational Study of Cooperative Binding to Multiple SARS-CoV-2 Proteins. *Sci. Rep.* **2021**, *11*, 16307. [CrossRef]
76. Azam, S.S.; Abro, A.; Raza, S.; Saroosh, A. Structure and Dynamics Studies of Sterol 24-C-Methyltransferase with Mechanism Based Inactivators for the Disruption of Ergosterol Biosynthesis. *Mol. Biol. Rep.* **2014**, *41*, 4279–4293. [CrossRef]

77. Rahman, F.; Tabrez, S.; Ali, R.; Akand, S.K.; Zahid, M.; Alaidarous, M.A.; Alsaweed, M.; Alshehri, B.M.; Banawas, S.; Dukhyil, A.A.B.; et al. Virtual Screening of Natural Compounds for Potential Inhibitors of Sterol C-24 Methyltransferase of Leishmania Donovani to Overcome Leishmaniasis. *J. Cell. Biochem.* **2021**, *122*, 1216–1228. [CrossRef]
78. Kwofie, S.; Broni, E.; Yunus, F.; Nsoh, J.; Adoboe, D.; Miller, W.; Wilson, M. Molecular Docking Simulation Studies Identifies Potential Natural Product Derived-Antiwolbachial Compounds as Filaricides against Onchocerciasis. *Biomedicines* **2021**, *9*, 1682. [CrossRef]
79. Lipinski, C.A. Lead- and Drug-like Compounds: The Rule-of-Five Revolution. *Drug Discov. Today Technol.* **2004**, *1*, 337–341. [CrossRef]
80. Kwofie, S.K.; Kwarko, G.B.; Broni, E.; Adinortey, M.B.; Wilson, M.D. *Molecular Informatics of Trypanothione Reductase of Leishmania Major Reveals Novel Chromen-2-One Analogues as Potential Leishmanicides*; IntechOpen: London, UK, 2021; p. 100594.
81. Kwofie, S.K.; Broni, E.; Asiedu, S.O.; Kwarko, G.B.; Dankwa, B.; Enninful, K.S.; Tiburu, E.K.; Wilson, M.D. Cheminformatics-Based Identification of Potential Novel Anti-SARS-CoV-2 Natural Compounds of African Origin. *Molecules* **2021**, *26*, 406. [CrossRef]
82. Islam, M.A.; Pillay, T.S. Identification of Promising Anti-DNA Gyrase Antibacterial Compounds Using de Novo Design, Molecular Docking, and Molecular Dynamics Studies. *J. Biomol. Struct. Dyn.* **2019**, *38*, 1798–1809. [CrossRef]
83. Veber, D.F.; Johnson, S.R.; Cheng, H.Y.; Smith, B.R.; Ward, K.W.; Kopple, K.D. Molecular Properties That Influence the Oral Bioavailability of Drug Candidates. *J. Med. Chem.* **2002**, *45*, 2615–2623. [CrossRef]
84. Sawale, R.T.; Kalyankar, T.M.; George, R.; Deosarkar, S.D. Molar Refraction and Polarizability of Antiemetic Drug 4-Amino-5-Chloro-N-(2-(Diethylamino)Ethyl)-2 Methoxybenzamide Hydrochloride Monohydrate in {Aqueous-Sodium or Lithium Chloride} Solutions at 30 o C. *J. Appl. Pharm. Sci.* **2016**, *6*, 120–124. [CrossRef]
85. van den Anker, J.; Reed, M.D.; Allegaert, K.; Kearns, G.L. Developmental Changes in Pharmacokinetics and Pharmacodynamics. *J. Clin. Pharmacol.* **2018**, *58*, S10–S25. [CrossRef]
86. Kwofie, S.K.; Annan, D.G.; Adinortey, C.A.; Boison, D.; Kwarko, G.B.; Abban, R.A.; Adinortey, M.B. Identification of Novel Potential Inhibitors of Varicella-Zoster Virus Thymidine Kinase from Ethnopharmacologic Relevant Plants through an in-Silico Approach. *J. Biomol. Struct. Dyn.* **2021**, *40*, 12932–12947. [CrossRef]
87. Banks, W.A. Characteristics of Compounds That Cross the Blood-Brain Barrier. *BMC Neurol.* **2009**, *9*, S3. [CrossRef]
88. Melo, G.D.; Goyard, S.; Fiette, L.; Boissonnas, A.; Combadiere, C.; Machado, G.F.; Minoprio, P.; Lang, T. Unveiling Cerebral Leishmaniasis: Parasites and Brain Inflammation in Leishmania Donovani Infected Mice. *Sci. Rep.* **2017**, *7*, 8454. [CrossRef]
89. Abreu-Silva, A.L.; Calabrese, K.S.; Tedesco, R.C.; Mortara, R.A.; Gonçalves Da Costa, S.C. Central Nervous System Involvement in Experimental Infection with Leishmania (Leishmania) Amazonensis. *Am. J. Trop. Med. Hyg.* **2003**, *68*, 661–665. [CrossRef]
90. Maia, C.S.F.; Monteiro, M.C.; Gavioli, E.C.; Oliveira, F.R.; Oliveira, G.B.; Romão, P.R.T. Neurological Disease in Human and Canine Leishmaniasis—Clinical Features and Immunopathogenesis. *Parasite Immunol.* **2015**, *37*, 385–393. [CrossRef]
91. Ali, N.; Ali, N.M.; Fariba, J.; Elaheh, H. The Efficacy of 5% Trichloroacetic Acid Cream in the Treatment of Cutaneous Leishmaniasis Lesions. *J. Dermatolog. Treat.* **2012**, *23*, 136–139. [CrossRef]
92. Momeni, A.Z.; Aminjavaheri, M.; Omidghaemi, M.R. Treatment of Cutaneous Leishmaniasis with Ketoconazole Cream. *J. Dermatolog. Treat.* **2003**, *14*, 26–29. [CrossRef]
93. Sakyi, P.O.; Amewu, R.K.; Devine, R.N.O.A.; Bienibuor, A.K.; Miller, W.A.; Kwofie, S.K. Unravelling the Myth Surrounding Sterol Biosynthesis as Plausible Target for Drug Design against Leishmaniasis. *J. Parasit. Dis.* **2021**, *45*, 1152–1171. [CrossRef]
94. Galvão, E.L.; Rabello, A.; Cota, G.F. Efficacy of Azole Therapy for Tegumentary Leishmaniasis: A Systematic Review and Meta-Analysis. *PLoS ONE* **2017**, *12*, e0186117. [CrossRef]
95. Weidner, S.; Kittelmann, M.; Goeke, K.; Ghisalba, O.; Zähner, H. 3′-Demethoxy-3′-Hydroxystaurosporine-O-Methyltransferase from Streptomyces Longisporoflavus Catalyzing the Last Step in the Biosynthesis of Staurosporine. *J. Antibiot.* **1998**, *51*, 679–682. [CrossRef]
96. Axelrod, J.; Daly, J. Phenol-O-Methyltransferase. *BBA-Enzymol.* **1968**, *159*, 472–478. [CrossRef]
97. Coque, J.J.R.; Alvarez-Rodríguez, M.L.; Larriba, G. Characterization of an Inducible Chlorophenol O-Methyltransferase from Trichoderma longibrachiatum Involved in the Formation of Chloroanisoles and Determination of Its Role in Cork Taint of Wines. *Appl. Environ. Microbiol.* **2003**, *69*, 5089–5095. [CrossRef]
98. Bustamante, C.; Ochoa, R.; Asela, C.; Muskus, C. Repurposing of Known Drugs for Leishmaniasis Treatment Using Bioinformatic Predictions, in Vitro Validations and Pharmacokinetic Simulations. *J. Comput. Aided. Mol. Des.* **2019**, *33*, 845–854. [CrossRef]
99. Cavaliere, F.; Fornarelli, A.; Bertan, F.; Russo, R.; Marsal-Cots, A.; Morrone, L.A.; Adornetto, A.; Corasaniti, M.T.; Bano, D.; Bagetta, G.; et al. The Tricyclic Antidepressant Clomipramine Inhibits Neuronal Autophagic Flux. *Sci. Rep.* **2019**, *9*, 4881. [CrossRef]
100. da Silva Rodrigues, J.H.; Miranda, N.; Volpato, H.; Ueda-Nakamura, T.; Nakamura, C.V. The Antidepressant Clomipramine Induces Programmed Cell Death in Leishmania Amazonensis through a Mitochondrial Pathway. *Parasitol. Res.* **2019**, *118*, 977–989. [CrossRef]
101. Manandhar, S.; Sankhe, R.; Priya, K.; Hari, G.; Kumar, B.H.; Mehta, C.H.; Nayak, U.Y.; Pai, K.S.R. Molecular Dynamics and Structure-Based Virtual Screening and Identification of Natural Compounds as Wnt Signaling Modulators: Possible Therapeutics for Alzheimer's Disease. *Mol. Divers.* **2022**, *26*, 2793–2811. [CrossRef]
102. Ahamad, S.; Kanipakam, H.; Birla, S.; Ali, M.S.; Gupta, D. Screening Malaria-Box Compounds to Identify Potential Inhibitors against SARS-CoV-2 Mpro, Using Molecular Docking and Dynamics Simulation Studies. *Eur. J. Pharmacol.* **2021**, *890*, 173664. [CrossRef]

103. Kant, V.; Ranjan, R.; Kumar, P.; Mandal, D.; Vijayakumar, S. *In silico* Screening, Molecular Dynamic Simulations, and in Vitro Activity of Selected Natural Compounds as an Inhibitor of Leishmania Donovani 3 - Mercaptopyruvate Sulfurtransferase. *Parasitol. Res.* **2022**, *121*, 2093–2109. [CrossRef]
104. Nagasubramanian, K.; Jha, S.; Rathore, A.S.; Gupta, K. Identification of Small Molecule Modulators of Class II Transactivator-I Using Computational Approaches. *J. Biomol. Struct. Dyn.* **2022**, 1–13. [CrossRef]
105. Zaki, A.A.; Ashour, A.; Elhady, S.S.; Darwish, K.M.; Al-Karmalawy, A.A. Calendulaglycoside A Showing Potential Activity against SARS-CoV-2 Main Protease: Molecular Docking, Molecular Dynamics, and SAR Studies. *J. Tradit. Complement. Med.* **2022**, *12*, 16. [CrossRef]
106. Steinbrecher, T.; Labahn, A. Towards Accurate Free Energy Calculations in Ligand Protein-Binding Studies. *Curr. Med. Chem.* **2010**, *17*, 767–785. [CrossRef]
107. Sun, Z.; Yan, Y.N.; Yang, M.; Zhang, J.Z.H. Interaction Entropy for Protein-Protein Binding. *J. Chem. Phys.* **2017**, *146*, 124124. [CrossRef]
108. Homeyer, N.; Gohlke, H. Free Energy Calculations by the Molecular Mechanics Poisson-Boltzmann Surface Area Method. *Mol. Inform.* **2012**, *31*, 114–122. [CrossRef]
109. Stuart, K.; Brun, R.; Croft, S.; Fairlamb, A.; Gürtler, R.E.; McKerrow, J.; Reed, S.; Tarleton, R. Kinetoplastids: Related Protozoan Pathogens, Different Diseases. *J. Clin. Investig.* **2008**, *118*, 1301–1310. [CrossRef]
110. Phan, T.N.; Baek, K.H.; Lee, N.; Byun, S.Y.; Shum, D.; No, J.H. In Vitro and in Vivo Activity of MTOR Kinase and PI3K Inhibitors Against Leishmania Donovani and Trypanosoma Brucei. *Molecules* **2020**, *25*, 1980. [CrossRef]
111. Rojas Vargas, J.A.; López, A.G.; Pérez, Y.; Cos, P.; Froeyen, M. In Vitro Evaluation of Arylsubstituted Imidazoles Derivatives as Antiprotozoal Agents and Docking Studies on Sterol 14α-Demethylase (CYP51) from Trypanosoma Cruzi, Leishmania Infantum, and Trypanosoma Brucei. *Parasitol. Res.* **2019**, *118*, 1533–1548. [CrossRef]
112. Baek, K.H.; Phan, T.N.; Malwal, S.R.; Lee, H.; Li, Z.H.; Moreno, S.N.J.; Oldfield, E.; No, J.H. In Vivo Efficacy of SQ109 against Leishmania Donovani, Trypanosoma spp., and Toxoplasma gondii and In Vitro Activity of SQ109 Metabolites. *Biomedicines* **2022**, *10*, 670. [CrossRef]
113. Alves, F.; Bilbe, G.; Blesson, S.; Goyal, V.; Monnerat, S.; Mowbray, C.; Ouattara, G.M.; Pécoul, B.; Rijal, S.; Rode, J.; et al. Recent Development of Visceral Leishmaniasis Treatments: Successes, Pitfalls, and Perspectives. *Clin. Microbiol. Rev.* **2018**, *31*, e00048-18. [CrossRef]